EROSION IN AN UPLAND MEDITERRANEAN ENVIRONMENT

AUTHOR:
ANNINA RUPPLI
GREBELACKERSTRASSE 33
CH-8057 ZURICH
08 – 058 – 364

SUPERVISOR AND FACULTY MEMBER:
PROF. DR. MARKUS EGLI
MARKUS.EGLI@UZH.CH
UNIVERSITY OF ZURICH

DEPARTMENT OF GEOGRAPHY
WINTERTHURERSTRASSE 190
CH-8057 ZURICH

DATE OF SUBMISSION:
29. SEPTEMBER 2016

Summary

Landscapes evolve over millennia and are strongly influenced by lots of different factors. For example, geological history, properties of parent rock material, effect of climate conditions, human impacts, vegetation, or time. To identify different evolutions in landscape development a reconstruction of soil formation helps to detect progressive phases with soil accumulation and regressive phases with soil erosion. A multi-methodological approach was chosen to achieve knowledge about long- and short-term soil formation. This time-split in erosion allows an identification of different temporal effects.

The Sila Massif in Calabria, southern Italy, is known as an erosive Mediterranean upland plateau. In this environment boulders denudate from the surrounding landscape. With surface exposure dating using cosmogenic ^{10}Be, the outcrop of these boulders can be set to an exposure age and an erosion rate over the exhumation can be derived. The sampled boulders on the plateau were exposed within the last 100'000-140'000 years, in which advanced and ceased denudation phases are detected. The long-term soil erosion rates of this phases can be linked to different climate conditions occurring in the Mediterranean environment. During the last interglacial phase with warm and wet conditions, the soil erosion rate was increased and the boulders' exposure accelerated. This interglacial period was followed by a cold and dry glacial phase, with tundra-like vegetation cover. In this time the erosion decreased and the boulders exposed slowly. Within the last 10'000 years, the climate has changed towards warmer and once again wetter conditions. This results in increased soil erosion rates, which is also detected on the boulders' denudation.

For short-term soil erosion rates the upper soil layer in the Sila Massif was analyzed on changes of the radionuclide plutonium. The results provide information about soil erosion of the last half century. It shows that human impacts affect the soil formation by increasing the erosion rates due to intense agriculture in the area until the year 2002. The detected short-term soil erosion rates are 25-50 times higher than the long-term rates, and are comparable to literature values from the same area. Furthermore, support the results from stable carbon isotope analysis the findings of this regressive phase in the Sila Massif by giving qualitative information as an indicator for soil erosion.

With the exposure ages of boulders and long- as well as short-term soil erosion rates, the surface development in the Sila upland plateau is reconstructed over the last hundred thousand years. It involves various climate conditions, which could be linked to different erosion rates, but are all part of a general soil regression in the upland Mediterranean area.

List of chapters and sections

List of figures

List of tables

Abbreviations

Al	Aluminum
Be	Beryllium
BP	before present
C_{tot}	total carbon
C_{inorg}	inorganic carbon
C_{org}	organic carbon
HCl	hydrogen chloride
$HF_{(aq)}$	hydrofluoric acid
LGM	last glacial maximum
Pu	Plutonium
SED	surface exposure dating
SOC	soil organic carbon
SOM	soil organic matter

1   Introduction

1.1   Landscape development reconstruction

The appearance of the earth's surface is affected by many factors and is the result of an interchange between different spheres like atmosphere, lithosphere, biosphere, and pedosphere. It is also known as the critical zone, where water and atmospheric gases move through the porous interface and shape the surface over time (U.S. NSF National Program, 2016). This shapening is the result of a.) the relief features, which are controlled by rock type, tectonics and overall geological history, b.) the properties of the soil and parent rock material, c.) the erosion of mobile material, d.) the effect of climate, e.) human impacts, f.) the vegetation cover and land use, and g.) time (Egli, et al., 2015). This leads to progressive and regressive evolutional phases, which can be put together as changing environmental conditions.

These progressive and regressive phases are strongly correlated to weathering and soil development. Furthermore, rock exposure in uplifted environments enhances the deepening of the weathering front and soil formation. The resulting profile thickness is a consequence of soil production less all losses due to denudation and organic matter decomposition. Soil formation and soil erosion leading to progressive and regressive development might change very abrupt due to catastrophic and natural events or the anthropogenic influences, e.g. changes in land-use or intensification of agriculture. Therefore, the development of soil and weathering of rocks is best regarded as discontinuous over time. (Johnson et al., 1987, Scarciglia et al., 2005, and Egli et al., 2015)

A soil profile shows vertical soil structure with increasing depth. Figure 1 shows the soil evolution with succession of progressive and regressive phases after Johnson and Whatson-Stegner (1987). It illustrates that in between time steps different phases of soil evolution can take place. The progressive evolutional phase is characterized by lager soil formation than soil erosion. The soil profile gains in depth. A bigger soil erosion than soil production results in a regressive phase, where the soil profile loses in depth. The erosion process, acting over temporal and spatial scales, is mainly driven by climate and tectonics. It leads to a rejuvenation of the soil and landscape surface and can expose less weathered material. (Egli et al., 2015)
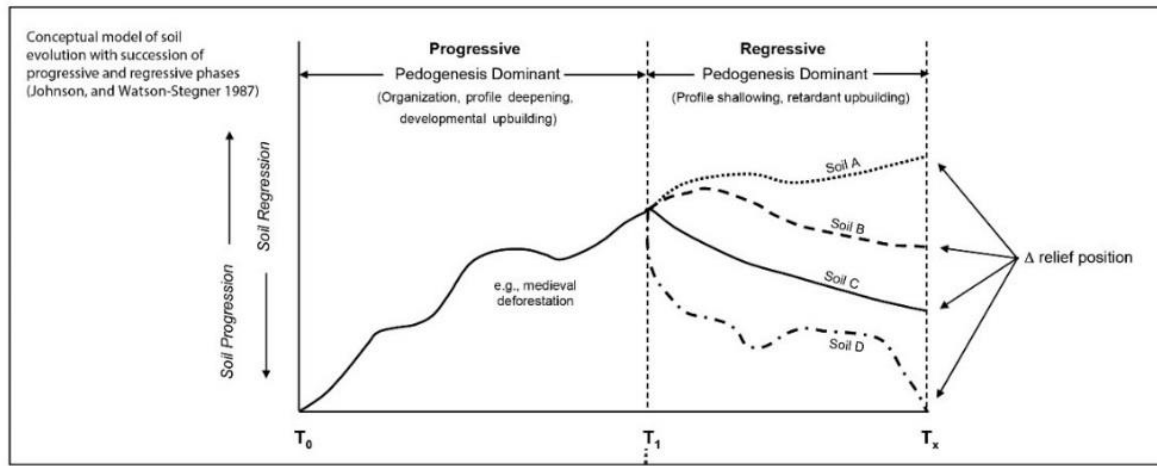
Figure 1. Soil evolution with progressive and regressive phases. (Johnson et al., 1987)

Landscape surfaces evolve over thousands of years and are known to develop in complex, non-linear ways. Soil profiles only reflect the developed surface at one point of time. It is unknown how fast the landscape surface evolved over time and whether phases with erosion or denudation were dominant. Although a possible development can be assumed from known conditions, it is only an assumption and not evidence based. Therefore, the reconstruction of a landscape over time helps to identify progressive and regressive phases in soil development. The researches of soil erosion rates are a common method to form an assumption about landscape development. (Egli et al., 2015)

1.2   Surface exposure dating using cosmogenic ^{10}Be

Schaller et al. (2002) as well as Egli et al. (2010) investigated in weathering mechanisms and erosion rates based on the distribution of in situ-produced ^{10}Be in quartz in soil profiles or river sediments. ^{10}Be, ^{26}Al, ^{36}Cl, ^{3}He, and other isotopes are built-up predictably with time in minerals exposed to cosmic rays. Measuring the concentration allows a determination of exposure to the atmosphere and is therefore a direct dating method. It has a possible upper age limit of tens of millions of years. (Ivy-Ochs et al., 2008, and Lal, 1988)

Cosmic rays constantly bombard the earth's surface. These rays produce beryllium (Be) by radiogenic nuclear reactions in quartz, which include the production by (1) high-energy spallation by nucleons, (2) neutron capture reactions, and (3) muon-induced nuclear disintegration (Lal, 1988). In all these reactions, the cosmic rays target an element in the mineral to build-up cosmogenic nuclides. In the case of ^{10}Be the target element is oxide O, which occurs in rocks as Silicon dioxide (SiO_2) also known as quartz. The production rate of ^{10}Be is altitude and latitude dependent, with a lower production rate at the equator and an increased production towards the poles, due to the earth's magnetic field and the

atmosphere. Additionally, the concentration of [10]Be rises significantly in higher altitudes and decreases towards sea level. Therefore, it is very important to note the precise sampling positions and altitude a.s.l. The cosmic ray flux is also reduced by shielding of surrounding hillslopes and mountains and results in a lower beryllium production. (Ivy-Ochs et al., 2008 and Lal, 1988)

The analyzes of quartz as weathered rock material in soils or as sediments in river is a reliable tool for erosion rates and therefore soil development. It has been tried to compare soil erosion rates over different time periods, but these studies lack in a distinction of soil erosion, from erosion as a general landscape process. Often the approaches only give a regional or large-scale signal and in most cases soil erosion cannot be discerned from other erosional processes. There is no precise information about special and temporal dynamics of soil formation and denudation and a new approach is needed to improve our understanding of weathering and erosion processes and their rates over time. (Egli et al., 2015)

1.3 Carbon isotopes and radionuclides as indicator for soil erosion

Soil erosion results not only in loss of material, but it also affects the components like soil aggregates, which shield soil organic carbon (SOC). The erosion of soil aggregates lead to mineralization or leaching of SOC and cause a decrease of carbon pool in this area (Schaub et al., 2009). A qualitative approach to investigate soil erosion is the analyzes of SOC content and the stable carbon isotope signature $\delta^{13}C$. Schaub et al. (2009), as well as Meusburger et al. (2013) proved this method to be a sensitive indicator of soil erosion processes on a mid-term scale. In several studies they compared undisturbed soil sites to such affected by erosion by measuring the stable carbon isotope and SOC.

A general increase in $\delta^{13}C$ in a soil profile reflects the decomposition of SOC. This process of decomposition in an oxic environment results in an increase of the heavier carbon isotope ^{13}C, because the lighter ^{12}C is preferred to be involved in chemical break-up processes, which only takes place in the upper soil. Stable soil conditions show a high correlation between $\delta^{13}C$ and SOC, whereas erosion weakens this correlation. This is because during soil erosion SOC is first to go into suspension in the form of small particles and is exported. The comparison to reference sites reflects the soil disturbance before a visible erosion is detectable. (Meusburger et al., 2013 and Schaub et al., 2009).

Recent studies by Ketterer et al. (2004), Alewell et al. (2014), Lal et al. (2013) and Zollinger et al. (2015) investigated the applicability of plutonium isotopes as a tracer for short-term soil erosion. In comparison to the isotopic method using carbon isotopes, this approach gives quantitative information by measuring the $^{239}Pu/^{240}Pu$ atom ratio in soil. Plutonium accumulation in soils occurs almost exclusively due to anthropogenic reasons. Atmospheric testing of nuclear weapons resulted in a peak fallout of this nuclear radionuclides in 1963/1964 (Ketterer et al., 2004). The origin is comparable to ^{137}Cs, which is an artificial radionuclide introduced into the environment via atmospheric nuclear weapon testing, or due to accidental releases from nuclear power plants like the Chernobyl reactor fire in 1986 (Ketterer et al., 2004).

The fallen out Pu is deposited on the surface by precipitation and strongly attaches to soil particles, where erosional processes lead to the removal and transport of Pu through the environment. The global distribution of Pu isotopes has been investigated by (Kelley et al., 1999). Since Pu has a long half-life of ^{239}Pu $t_{1/2}$ = 24110 yr, and ^{240}Pu $t_{1/2}$ = 6563 yr, it is still available in soil samples for measurements and is therefore a suitable method for investigating short-term soil redistribution of 25-60 years. An undisturbed soil should show a high accumulation of Pu in the upper 10 cm, because the radionuclides are preferentially attached to soil organic matter (SOM). Therefore, one can assume that due to erosion the upper soil particles are removed and a lower Pu content is detectable on erosive sites. (Lal et al., 2013, Zollinger et al., 2015, and Ketterer et al., 2004).

The Pu may also be influenced by vegetation, because radionuclides can be absorbed by plant surfaces or taken up by roots and are not released into the soil until the plant dies (Zollinger et al., 2015).

1.4   Research questions and hypotheses

This master thesis is based on a research project by Markus Egli (University of Zurich), and Fabio Scarciglia (University of Calabria). The project focuses on the exhumation rates in low-gradient landscapes by analyzing the Be content in boulders. Therefore, the thesis follows the main research questions and hypothesis of "Project Beryllium". Its idea is to investigate soil erosion of different time steps to reconstruct previous phases of landscape development. Boulder fields, consisting of granitoid and gneissic terrains, growing from gentle landforms may be characterized and can be seen as a key for deciphering temporal evolution of soil erosion rates.

Since it can be assumed that rock boulders have a higher physical resistance to weathering, they are not as easily eroded as the surrounding material. Hence, the hypotheses are:

(1) rock boulders are harder than weathered material and must outgrow in an eroding landscape in comparison to its surrounding, (2) the speed of their outgrowth is an indicator of the surrounding surface erosion, (3) since the eroding landscape denudates the boulders, they are exposed to cosmic rays, which produce beryllium in the quartz of the granitoid rocks. The longer the exposure the higher is the cosmogenic ^{10}Be. (4) Therefore, the ^{10}Be content must be highest on top of each boulder and decrease towards the soil surface as a result of the continuous outgrowth and denudation from top to bottom. By measuring this ^{10}Be content at different heights along a rock boulder the age of exposure can be derived.

Surface exposure dating gives a quantitative information about the boulder exhumation in the study area. Another methodological approach can be done with $^{239+240}$Pu and δ^{13}C in the soil close to the exposed boulders.

Pu measurements on the reference site should show, that the fallen out radionuclide of the past are mostly accumulated in the upper part of the soil and decrease with soil depth. In disturbed areas, the upper soil with attached Pu is eroded and the Pu therefore significantly lower in comparison to the reference site.

The expectance for the control site is a high correlation of δ^{13}C signature and SOC. The disturbed areas should have a lower correlation, since the erosion process lowers the SOC, which generally also results in a lower total carbon content (C_{tot}). However, this approach will only give qualitative information about soil erosion in this area.

The following research questions build the basis of this master thesis:

1. How did soil develop over time – can progressive and regressive phases be detected?
2. Can the surface lowering rates be related to climate changes and / or tectonic phases?
3. Is the large-scale erosion comparable with short-term erosion?

2   Study area

2.1   Geographical setting

The study area is located in the region of Calabria in the southern part of Italy. It belongs to the ground area of the Sila National Park which is situated in the center of Calabria belonging to the provinces of Cosenza, Crotone and Catanzaro. The Sila National Park extends over an area of 73.7 ha between the cities of Cosenza in the west and Crotone in the east of Calabria and was founded in 2002. The National Park is divided into the following three sectors – Sila Grande, Sila Piccola and Sila Greca. (Ente Parco Nationale della Sila, 2016)
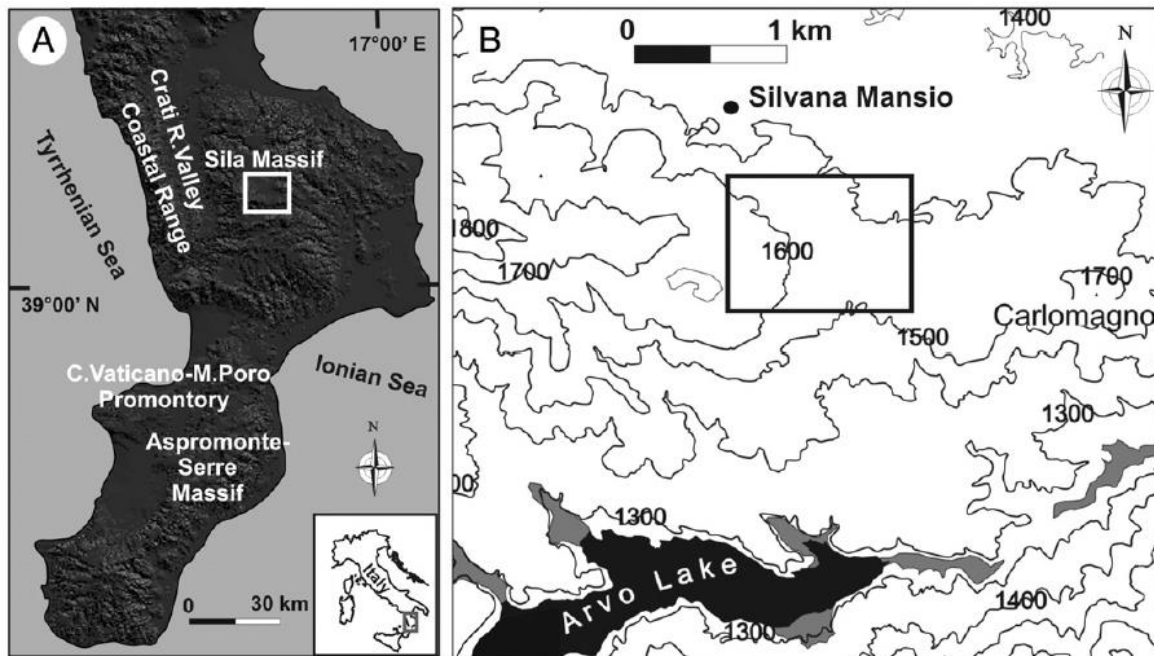
Figure 2. Location of the study area in the Sila Massif, Calabria, southern Italy. (Scarciglia et al., 2012)

As shown in figure 2 the investigation area is in the Sila Massif on a high plateau at an elevation of 1570 m a.s.l. close to the village of Silvana Mansio. The surrounding is characterized by a gentle landform of wide soft hilly ground bordered by steep slopes which represent remnants of old planation landforms shaped since the Pliocene to the Pleistocene (Egli et al., 2015).

2.2   Climate and vegetation conditions

The study area in the Sila Massif has according to Köppen (1936) a typical upland Mediterranean climate. The temperature in this humid climate is characterized by mean monthly temperatures ranging from -1°C in January to 16-18°C in August and a not particularly prolonged dry summer with a mean maximal temperature of 22°C. The closest meteorological station is on top of Scuro Mountain at an elevation of 1720 m a.s.l., about 10 km from Silvana Mansio. The associated climate graph is shown in figure 3.

	jan	feb	mar	apr	may	jun	jul	aug	sep	oct	nov	dec
Precipitation [mm]	93.2	87.4	68.8	58.1	49.5	37.1	21.4	34.4	50.6	93.6	107.5	108
Average Temp [C°]	0.1	0.1	1.6	4.5	9.5	12.8	15.8	15.8	12.9	8.6	4.8	1.5
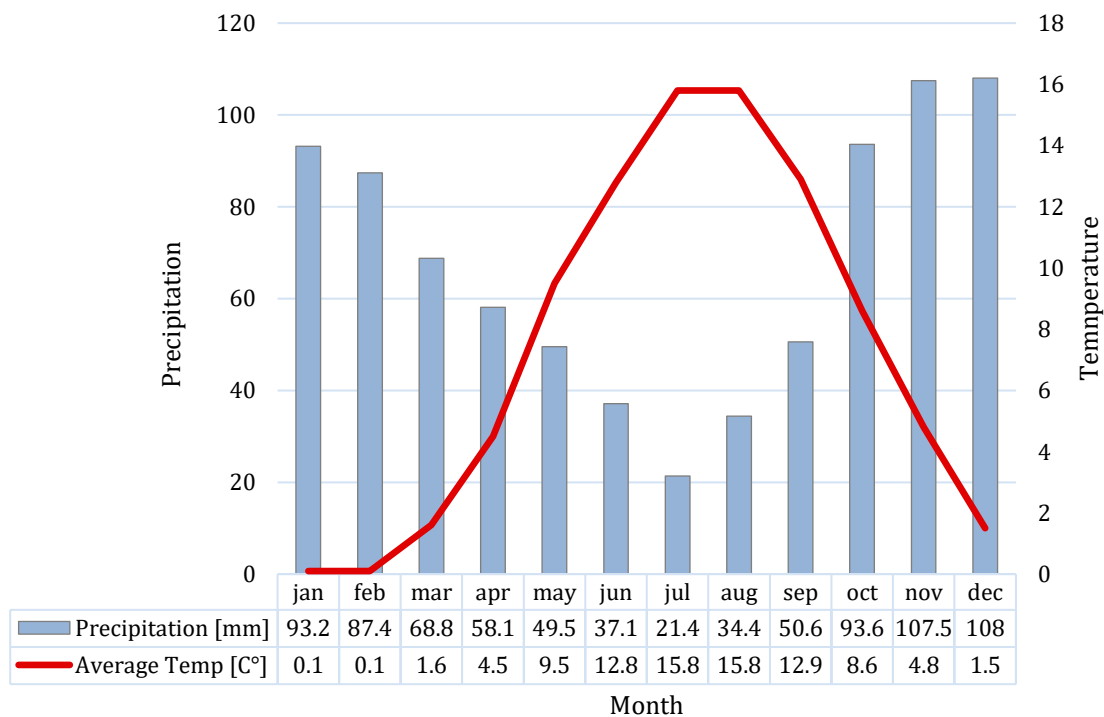
Figure 3. Cilmate graph Scuro Mountain, Sila Massif.

According to Lulli et al. (1992), Colacino et al. (1997), and Versace et al. (1989) the mean precipitation ranges form 1400-1600 mm per year. Precipitation falls mostly throughout the fall-winter season, as snow above 1400-1600 m a.s.l., and persists up to 6 months. The mean annual precipitation and temperature influence the leaching factor, which is due to the high precipitation rate in the Sila Massif among the highest in Europe. (Le Pera et al., 2000, and Lulli et al., 2000)

The predominant vegetation mostly consists of a mixed forest out conifers like larch or pines and broadleaf trees like beeches. The herbaceous layer is dominated by fern and grassland. This vegetation is the result of the progressive re-naturalization in the Sila Massif (Scarciglia et al., 2005).

2.3 Geological conditions

The southern part of Italy is based on two geological structured chain segments, the Calabrian-Lucanian Apennines in the north and the Calabria-Peloritani Arc in the south. The Sila Massif in the south forms the highest tectonic unit of the southern Italy fold-trust belt, known as the Calabrian Arc. The area is tectonically active, whereas high uplift rates formed the landscape of plateaus bordered by steep slopes where the average estimate of uplift rate seems to remained constant over the last millenium (Perri et al., 2014, and Olivetti et al., 2012).

The Sila Massif consists of Palaeozoic intrusive and metamorphic rocks, locally with unmethamorphosed, Mesozoic sedimentary cover. The Palaeozoic metamorphic basement rocks consists mainly of gneiss, amphibolite, schist and phyllite, whereas the intrusive granitoid rock consist of predominant K-feldspar, plagioclase, quartz, biotit, and muscovite, and is widespread on the older planation surfaces of the Sila Massif. They emerge in the study area on the Sila plateau as a result of an eroding landscape. The major phases of Pleistocene tectonic uplift, which increased the elevation of the Sila plateau from the base level, can be seen as a reliable time mark for the onset of the main erosion phases. Due to the investigation of the main river valleys by Olivetti et al. (2012) the evolution of the Sila landscape is suggested by uplift phases. Scarciglia (2015) describes the landscape evolution of the plateau as follows: The low-relief landscape, which developed in the Miocene, was lifted during the late Pliocene and early Pleistocene and isolated the relict summit landscape. The next phase in early and middle Pleistocene influenced the landscape development in three ways. (1) It had a more extensive uplift, (2) an increase in local relief, and (3) a progressive isolation of the former landforms. Followed by this tectonic uplift the landscape was formed further by strong river incisions and severe erosion. (Scarciglia et al., 2005, Olivetti et al., 2012, Perri et al. 2014, and Scarciglia, 2015)

Figure 4. Clear exposure lines show the ongoing denudation of boulders in the Sila upland Plateaus. (Foto: A.Ruppli)

This leads to the exhumation of boulders ranging from about 0.3 m to 3-4 m in diameter, forming large boulder fields and castellated inselberg-like landforms close to Arvo Lake. On the highest plateaus they often lie at the topographic surface and are subject to further chemical, physical and biological weathering processes. The exhumation phases can be detected on the boulders surface, since clear lines with change of color occur as an indicator of weathering processes shown in figure 4. The exhumation is furthermore favored by the typical upland Mediterranean climate conditions in combination with the tectonic activity. (Egli et al., 2015, and Scarciglia et al., 2005)

3   Methods

To compare long-term erosion with mid- and short-term erosion different methods are required. A multi-methodological approach using isotopes is done to compare the landscape development from decades to millennia.

The exhumation of boulders takes thousands of years and therefore the surface exposure dating reflects the long-term erosion and landscape formation of the area in the Sila Massif. Another method sampling boulders is the relative dating technique using the Schmidt-Hammer. It gives a qualitative information about the weathering conditions of the boulder surface close to the ^{10}Be sampling point. It can be used as a crosscheck of the exposure age, calculated with the ^{10}Be concentration. The soil samples are used to investigate the short- and mid-term erosion in the area. The comparison should once more be a helpful tool to reconstruct the development. Where the results of the carbon isotope analysis give a qualitative information about soil erosion, the Pu measurements have a quantitative aspect about recent soil distribution processes.

3.1   Field work

All samples were taken in the investigation area in the Sila Massif. Figure 5 shows the exact position of the sampling sites in the field. Overall 12 rock samples 60 soil samples have been collected from October 27th until October 30th 2015.

Figure 5. Sample sites in the investigation area. Boulder sample sites in yellow, soil sample sites in orange.

3.1.1 Rock sampling

Granitoid boulders are ideal for the investigation of cosmogenic [10]Be, since this is produced in the quartz of the granites. The chosen sample area is a wide boulder field on a relatively flat surface on an upland plateau. The boulders had to fulfill following criteria to be chosen as sampling sites:

- they should be exposed at least 2 m above soil surface to get a decent disparity in [10]Be concentration
- they should have been continuously exposed in the same position and not be shifted as far as it can be prejudged in the field
- they should have undergone only minimal surface weathering or erosion because highest [10]Be production takes place close to the boulder's surface.
- they should have a good access for sampling out of practical reasons

Satisfying the criteria three boulders (Bo 1, Bo 2 and Bo3) were chosen to be an ideal sampling site in the boulder field, located in figure 5. They are situated within a distance of maximal 120 m to each other and one can assume they are exposed to the same weathering conditions.
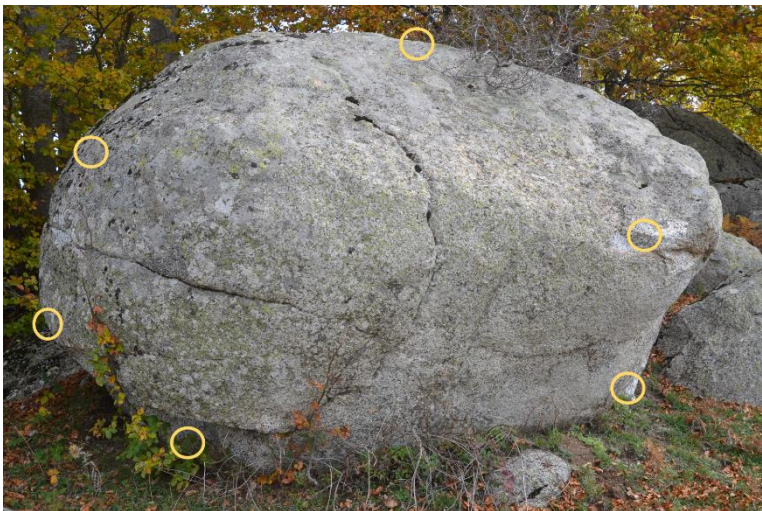
Figure 6. Rock sampling positions (exemplary on Bo 1) on different levels along the boulders surface. (Foto: A.Ruppli)

Boulder 1 (Bo 1) (see figure 6) has a total height of 225 cm. Three samples were taken in 2014 and 3 more in 2015 giving a boulder profile from 10 cm above soil surface up to 225 cm at the very top of the boulder, listed in table 1. During sampling it became clear that this boulder is totally exposed and only few centimeters of the rock are under the soil surface.

Therefore, the results of Bo 1 should give an overview from bottom to top of the whole boulder. Boulder 2 (Bo 2) was the biggest boulder in this area. It has a total height of 6 m above soil surface, is 5 m wide, and 8 m long. The assumption is very close that this rock has not moved over time, due to the fact that it might have a weight of over 63 tons (calculated with a density of 6.2g/cm³ for granite by Lal, 1988). In comparison to Bo 1, this boulder is not yet fully exposed. Rock samples were taken along the surface from bottom to top with 50-200 cm in between. For this boulder a rock sample under the soil surface could be taken to measure the pre-exposure accumulation of [10]Be.

Boulder 3 (Bo 3) is the smallest sample site with 2 m above soil surface. It is located 1.5 m next to Bo 1 and is like Bo 2 partially exposed. Hence, a sample under the soil surface could be taken. This boulder shows the smallest profile, because it was only sampled on three heights along the rock surface. Both boulder (Bo 1 and Bo 3) were partially under a grove with a slightly tilted soil surface level. A visible impression of all sampled boulders is shown in figure 7.

Table 1. Sampling heights in cm for all taken samples in the study area since 2014.
*Bo 2 and Bo 3 are assumed to continue under the soil surface. *Samples taken in 2014.*

	Bo 1	Bo 2	Bo 3
		560	
		460	
	224	240	
			170
sampling height in cm	128	135	120
	108		
	76*		
	25*	30	
	10*		
		-20	-20

Granite rock is a known as a very hard material. Therefore, a sampling time of almost one hour per sample had to be taken into account. The time issue and the fact, that granitoid rocks are heavy material reduces the possibility of taking to many samples at once. For each chosen boulder is was deliberated on how many and where exactly the rock samples should be taken. The sampling was achieved with a stone saw, hammer and chisel to cut pieces from the rock surface. Samples within a depth of 5-10 cm is favored, since the ^{10}Be accumulation decreases with depth towards the stone core. To get a suitable amount of quartz, 1-2 kg rock per sample was taken from the different surface levels.

A sample form for each rock sample was filled out with the following information: Latitude, Longitude, Altitude, Exposure, Dip, Shielding, Sample thickness, rock type, and sampling technique. An example for a ^{10}Be-dating form can be found in the appendix. The above mentioned information is furthermore important to calculate the exposure age, explained in the chapter about analysis of SED.

Figure 7. Sample boulders in the study area. Top left picture Bo 1, top right Bo 3, bottom Bo 2. (Fotos: A. Ruppli)

With the analyzes of cosmogenic [10]Be an absolute exposure dating can be approached. To get a first field impression on the rock hardness and its weathering status of the surface a relative dating technique was used. The Schmidt-Hammer is a portable tool, designed to measure the surface strength by recording the rebound of a spring-loaded bolt when hitting a surface (Egli et al., 2015).

It represents the degree of weathering and linked to that the exposure of the surface. Denudated rocks are exposed to chemical and physical weathering, which results in a lower rebound value (r-value) due to slightly fractured surface conditions. Thus, the Schmidt-Hammer can be used to crosscheck the exposure age based on cosmogenic [10]Be content and was applied as close as possible to the rock sampling spot. To get a reliable average r-value per sample, 15-20 replicas were taken to minimize possible error sources such as lichen cover on the boulders surface, hairline cracks and degree of humidity within the boulder, slightly angled position of the Schmidt-Hammer, and unstable measuring position.

3.1.2 Soil sampling

Soil samples for erosion analysis of $\delta^{13}C$ and $^{239+240}Pu$, were also taken in the same study area. Both methodological approaches could be done with the same soil sample. The criteria for soil sampling sites were not as high as for rock sampling. Since the study area was on a gentle landform and therefore relatively flat, the study sites with disturbed soil needed to have at least a minimal slope angle of 5°.

Figure 8. Soil sampling at the reference site with a core sampler. (Foto: A.Ruppli)

One reference site (R) was chosen on a flat surface with no slope angle and therefore with no significant exposure to one direction. The site R had a predominant grass vegetation as seen in figure 8. In approximately 100 m distance to the reference site two investigation sites (A and B) were chosen (see figure 5). Site A was a little bit more uphill with a slope angle of 7°. It had an exposition to 0° north with a vegetation cover of grassland and moss. Site B had a slight bigger slope angle with 10° and was exposed to 330° north. The vegetation was as well grassland and moss. The study sites A and B differed on only 20 m to each other.

Soil cores with only topsoil material were taken by a core sampler. They referred to a depth of 0-15 cm from soil surface. For each site (R, A, and B) four replicas were extracted to minimize outlier values.

3.2   Lab work and data analysis for boulder samples

3.2.1   Rock sample preparation

The boulder samples were prepared for the SED using ^{10}Be at the laboratory of University of Zurich. To analyze the ^{10}Be amount, the rock sample had to be separated into its components. Granitoid rocks consist of predominant K-feldspar, plagioclase, quartz, biotit, and muscovite (Scarciglia et al., 2005), but only quartz is of further need, since ^{10}Be is produced in this component. The preparation and processing steps follow the geochronology laboratory methods from University of Zurich by (Egli et al., 2013).

As a preparation step, the rock samples were crushed into piece by a rock crusher. A fraction of 0.6-0.25 mm is needed for further procedures. The sample is crushed and sieved several times until about 0.5 kg of the appropriate fraction is collected. The remaining rock fraction >0.6 mm and <0.25 mm is stored as back up material for future measurements if necessary. Next the crushed sample is mixed with nitrohydrochloric acid and left resting for 12-24 hours to dissolves carbonates and iron oxides without losing any quartz. Froth floatation is used for separating feldspar particles from quartz, which have overlapping densities (Herber, 1969). Kawatra (2011) describes froth floatation as a highly versatile method for physically separating particles based on differences in the ability of air bubbles to selectively adhere to specific mineral surfaces in a water slurry. This method is bases on differences in wettabilities, in which eucalyptus oil is induced as a chemical treatment. It changes the hydrophobicity of feldspar particles in such way, that they attached to air bubbles and float to the surface. The separation is carried out by decantation. The hydrophilic particles like quartz shows less tendency to attach to the bubbles and will deposit at the bottom. With this chemical method most of the feldspars is removed and the leaching process with hydrofluoric acid ($HF_{(aq)}$) to dissolve all carbonate can be reduced in time.

For leaching the sample is treated with no higher than 4% $HF_{(aq)}$, otherwise quartz will be suspended as well. This mixture is left on the shaker for 48 hours. This step is repeated once or twice depending on the dissolving progress. After this process the remaining sample consists of pure quartz and is rinsed with ultra-pure water and dried in the oven at 80°C. The pure quartz is now needed to be dissolved and only the isotope ^{10}Be is extracted from the sample. A carrier of $^{9}Be(NO_3)_2$ solution in 40% $HF_{(aq)}$ acid is given to each sample to dissolve the quartz at 150°C. In a chemical procedure of cation exchange column chemistry Al is further separated from the dissolved sample using a HCl solution. The Be sample is transferred to a quartz crucible and dried at 70°C. Closed with a quartz lid, the samples are left to calcinate for 2 hours at 850°C. Before measuring in the AMS at ETH, Zürich, the sample needs to be mixed with Cu powder and pressed into an accelerator target.

3.2.2 Analysis for SED and surface lowering rates

By measuring the ratios relative to a standard material, the accelerator mass spectrometry is used to determine concentrations of cosmogenic nuclides such as [10]Be (Ivy-Ochs et al., 2008). The Laboratory of Ion Beam Physics of the Swiss Federal Institute of Technology ETH, Zürich, provided the measurements using an AMS, Tandy with 07KNSTD as standard. The ratio of [9]Be/[10]Be, and the [10]Be concentration in atoms per gram sample was measured. Within this result a correction was needed, since the carrier [9]Be naturally contains a little amount of [10]Be, which falsifies the result. For correction a blank measurement with only carrier was analyzed and the blank [10]Be concentration was subducted from the first measurement to get a final result with the [10]Be concentration for each boulder sample. The results have been normalized to the in-house secondary Be-10 standard S2007N with a nominal value of [10]Be/[9]Be = 28.1 x 10^{-12} (Christel, 2016).

For calculating the exposure age, the production rate of [10]Be, and consequently the cosmic ray-flux is essential (Balco et al., 2008). If a site is partially shielded by the surrounding topography or by a nominally infinite dipping surface surrounding the sample, a correction in production rate has to be calculated, which can be done with the shielding correction by CRONUS per sampling position. The exposure age is then calculated using the CRONUS calculator for exposure age provided by the Cosmogenic Nuclide Lab (2016). Table 2 by Balco et al. (2008) shows measurements and observations needed to calculate the exposure age. With the age of different levels above ground, the surface lowering rate is calculated.

Table 2. List of measurements and observations from field and lab work to calculate the exposure age according to CRONUS, modified after Balco et al. (2008).

Field	Units	Comments
Sample name	Text	
Latitude	Decimal degrees	South latitudes are negative
Longitude	Decimal degrees	West longitudes are negative; longitudes should be between -1800 and 1800
Elevation	m a.s.l. or m (hPa)	Sample elevation can be specified as either meters above sea level or as mean atmospheric pressure at the site.
Sample thickness	cm	
Sample density	g/cm3	
Shielding correction	between 0 and 1	Ratio of the production rate at the obstructed site to the production rate at a site at the same location and elevation with flat surface and clear horizon.
Rock erosion rate	cm/yr	The erosion rate of the sample surface, to be taken into account when computing the exposure age.
Nuclide concentrations	atoms/g	[10]Be concentrations in quartz in the sample. Should account for laboratory process and carrier blanks
Uncertainties in nuclide concentrations	atoms/g	1-standard error analytical uncertainties in the measured nuclide concentrations. Should account for all sources of analytical error, including AMS measurement uncertainty

3.3   Lab work and data analysis for soil samples

3.3.1 Soil sample preparation

The taken soil cores from the Sila Massif of 0-15 cm depth, were divided into sections of 3 cm soil material. This equals in a vertical soil profile of five samples in depth with four replicas per sample site. In the laboratory the soil samples were prepared for different measurements, including general soil parameters, carbon isotope analysis, and radionuclide analysis.

The samples were dried in the oven at 60°C for 16 hours and the dry material sieved at 2 mm to extract the coarse material like stones and roots. Next the fine soil < 2 mm was ground using a planetary mill (Fritsch, Pulverisette 5) and again sieved using smaller meshes, because for further procedures only fine material < 125 µm was needed.

3.3.2 Soil Carbon Content

Using a C, H, N Elemental Analyzer the total carbon content (C_{tot}) of each sample could be determined. The same analysis serves also the hydrogen and nitrogen content of the soil, which was of no interest for the thesis. Approximately 2-3 mg per soil sample was weighed into tin capsules and sent to the CHN Analyzer in the Department of Biology at University of Zürich.

The CHN instrument uses high temperature combustion to remove the element from the material (Egli et al., 2013). In this process the sample is heated up to 550°C under the influence of oxygen and releases the oxygenates CO_2, NO_x and H_2O, which are measured by a non-dispersive infrared absorption detection system and with adjustments the weight percent carbon, hydrogen and nitrogen is displayed (Egli et al., 2013). The C result represents the C_{tot} content, which is composed of C_{org} and C_{inorg}. The soil organic carbon (SOC) content is further used with the isotope signal $\delta^{13}C$ as a function of soil depth to indicate erosion and mixing processes in soils. (Schaub et al., 2009)

3.3.3 Carbon isotope analysis

For qualitative erosion, the soil samples were analyzed for stable carbon isotopes ^{13}C. Therefore, the samples were weighted into tin capsules according to its measured carbon content by the CHN analysis. Each sample should contain about 300 µg C, hence 1-30 mg soil per sample was prepared for measuring. The $\delta^{13}C$ analysis was accomplished at University of Basel, using a EA-IRMS, Elemental Analyzer Isotope Ratio Mass spectrometer, which follows a Sercon Integra2 system (Sercon Ltd., Crewe, UK) with EDTA and USGS41 as standards. Like for CHN analysis, the sample is converted to CO_2 with the presence of oxygen, which is then measured at the detector of the mass spectrometer.

3.3.4 Radionuclide analysis

Plutonium could be measured from the already prepared samples described in chapter 3.3.1. Of each sample 10-15 g were weighted into glass vials and dry-ashed at 550°C for 24 hours to remove all organic matter. The samples were shipped to Prof. M. Ketterer's group at the Metropolitan State University of Denver CO, USA. Approximately 5-6 g per sample were analyzed for 239/240 Pu ratio. The remaining soil has been archived for potential re-analysis. The chemical procedure for measuring the plutonium were adapted from those reported in (Ketterer et al., 2004). The samples were analyzed using a Thermo X Series II quadrupole ICPMS system. The control samples consisted of Pu-devoid sandstone and samples of known Pu.

With the results the according Pu inventory was calculated based on the following equation (1):

$$I = z \times \rho \times Pu \tag{1}$$

where I = inventory (Bq/m²) is calculated for each sample depth (= z cm) with ρ = soil density (for calculation reasons in kg/m³), and Pu = ratio of $^{239/240}$Pu (Bq/kg). The results per sampling depth were then added up together to get the inventory per soil profile for all four replicas and an average inventory per sample site.

Soil erosion rates were calculated with the equations (2) and (3) by comparison of the isotope inventory for the eroding sites ($I_{A,B}$) to the reference site (I_R), which is then converted into soil redistribution rates. For the reference soil no erosion is expected.

In a first step, the % inventory loss (X) is calculated according to equation (2):

$$X = 1 - \left(\frac{I_{A,B}}{I_R} \right) \tag{2}$$

In equation (3) the loss is converted into soil erosion rate:

$$\varepsilon = \left(\frac{X \times \dfrac{z}{t - t_0}}{1000} \right) \times \rho \times 10^4 \tag{3}$$

where ε = erosion rate (t/ km²/yr), ρ = soil density (g/cm³), z = soil depth, t = year of sampling and t_0 = 1963, due to the fact, that thermonuclear weapon testing with Pu had its peak in this year.

In the equation the rate was multiplied with 10^4 to get an erosion rate in the unit t/ km²/yr. The erosion rates were calculated for each sampling depth and then average rates for each investigation site was calculated.

4 Results

4.1 Surface exposure age using [10]Be

The exposure ages of all sampled boulders were calculated with CRONUS online (Cosmogenic Nuclide Lab, 2016), in which some variables, like rock erosion rate, have to be estimated. To get a minimum and maximum exposure age, the rock erosion rate was varied for selected samples with a minimum erosion of 0.0001cm/yr and a maximum erosion of 0.0005cm/yr. In general, the calculated maximal exposure ages have a higher uncertainty than the calculated minimal exposure ages.

With the exposure ages of different levels above soil surface, the surface lowering rate could be calculated. This values give information about an average lowering of the surface in between the calculated exposure ages, which can include big time steps. Positive values stand for erosion rate, whereas negative values are meant to be accumulation rates.

In table 3 the basic information for all boulder sites are listed. These are identical for all taken samples of the same boulder, except the sample thickness. This value is mostly between 2-3 cm, only for the two samples taken underneath the soil surface each account 9.5 cm, because of an addition factor for covered samples.

Table 3. Basic information for rock samples in the investigation area.

Sample boulder	Latitude (°N)	Longitude (°E)	Elevation (m a.s.l.)	Thickness (cm)	Min. rock erosion rate (cm/yr)	Max. rock erosion rate (cm/yr)
Bo 1	39.281	16.539	1572	2 - 3	0.0001	0.0005
Bo 2	39.281	16.540	1572	2 - 9.5	0.0001	0.0005
Bo 3	39.281	16.539	1572	2 - 9.5	0.0001	0.0005

Bo 1 represents the totally exposed boulder from bottom to top with six taken samples along the surface listed in table 4.

The sample closest to the soil surface shows the highest exposure age with 80'000 years. The exposure ages between the sample heights of 25-128 cm vary from 40'000-78'000 years. The highest taken sample spot at 225 cm heights is dated to be 24'000-25'000 years exposed, which is the lowest exposure age for this boulder. Some samples show similar exposure ages even though they are not at the same level above soil surface. But one can see that the three highest taken samples have lower exposure ages according to the [10]Be calculations as illustrated in figure 9. The sample closest to the soil surface has the highest exposure age.

Table 4. Surface exposure dating of boulder 1 with minimum and maximum ages according to CRONUS.

	Bo1/10	Bo1/25	Bo1/76	Bo1/102	Bo1/128	Bo1/225
Shielding correction	0.49	0.498	0.558	0.879	0.613	0.999
^{10}Be (atoms/g)	5.01E+05	2.84E+05	3.44E+05	6.90E+05	3.07E+05	3.02E+05
Measurement error (%)	5.90%	7.40%	9.90%	4.06%	4.18%	5.50%
Min. exposure age (yr)	79'876 ± 6214	41'590 ± 3790	50'003 ± 5814	65'610 ± 4429	40'248 ± 2674	24'118 ± 1798
Surface lowering (mm/yr)					-0.008	-0.06
Max. exposure age (yr)				77'961 ± 11'337	42'916 ± 5307	24'948 ± 3000
Surface lowering (mm/yr)					-0.006	-0.054

Since the samples show very inconsistent results in exposure age, the surface lowering was calculated for the three highest taken samples, which show a clear trend. The surface lowering rate between Bo1/102 and Bo1/128 is very low with - 0.006 to -0.008 mm/yr. Between Bo1/128 and Bo1/225 it accounts -0.054 to - 0.060 mm/yr. This results have negative values, which indicate an accumulation of soil. They give a rough estimation of the surface development based on time steps of 15'000 and 35'000 years.
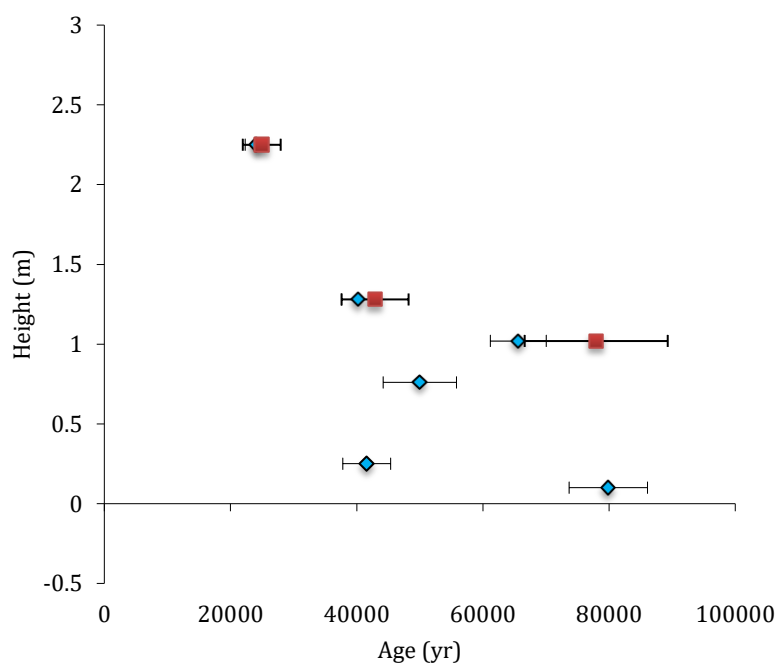
Figure 9. Exposure ages of boulder 1 in correlation to sample heights.
Minimal ages in blue and maximum ages in red.

Compared to the first boulder the second boulder shows very consistent exposure ages according to the calculations, shown in table 5. The sample at 135 cm height did not get any value in the AMS, therefore, only five samples provide information for this boulders exhumation. The exposure ages increase with higher levels above soil surface. The lowest sample above soil surface at a level of 30 cm have an age of around 10'700-11'000 years. Followed by the sample at 240 cm, which is calculated to an age of approximately 32'000 years. Within 2 meters along the boulders surface the exposure age increases to 92'000-127'000 years at 460 cm. At the highest sampling point of 560 cm above soil surface the exposure age accounts 100'000-143'000 years.

Table 5. Surface exposure dating of boulder 2 with minimum and maximum ages according to CRONUS.

	Bo2/-20	Bo2/30	Bo2/240	Bo2/460	Bo2/560
Shielding correction	0.724	0.614	0.771	0.614	0.972
^{10}Be (atoms/g)	1.38E+05	6.94E+04	3.01E+05	7.09E+05	1.13E+06
Measurement error (%)	5.20%	20.00%	4.90%	3.90%	3.90%
Min. exposure age (yr)	13'759 ± 1400	10'724 ± 2234	31'145 ± 2219	92'286 ± 6285	99'636 ± 6883
Surface lowering (mm/yr)	-0.165	0.103	0.036	0.136	
Max. exposure age (yr)	15'316 ± 1637	10'988 ± 2546	32'681 ± 3978	126'678 ± 23'350	142'727 ± 28'681
Surface lowering (mm/yr)	-0.116	0.097	0.023	0.062	

As mentioned in the chapter 3 about field work, this boulder was not yet fully exposed and rock samples still covered by soil could be taken. The sample at -20 cm was calculated to be a little longer exposure to cosmic rays with an age of 14'000-15'000 years, than the sample taken at 30 cm above soil surface. This exposure age is based on the pre-accumulation of ^{10}Be, which forms through cosmogenic waves penetrating underneath the soil surface. The two highest taken samples Bo2/460 and Bo2/560 show a range between minimal and maximal exposure age of 34'000 and 43'000 years, respectively, whereas samples closer to the soil surface have a closer range of 5'000 years between minimal and maximal age. A phases with relatively high lowering rates of approximately 0.1 mm/yr alternate to a low surface lowering of 0.03 mm/yr and back to a high rate of 0.062-0.136 mm/yr.
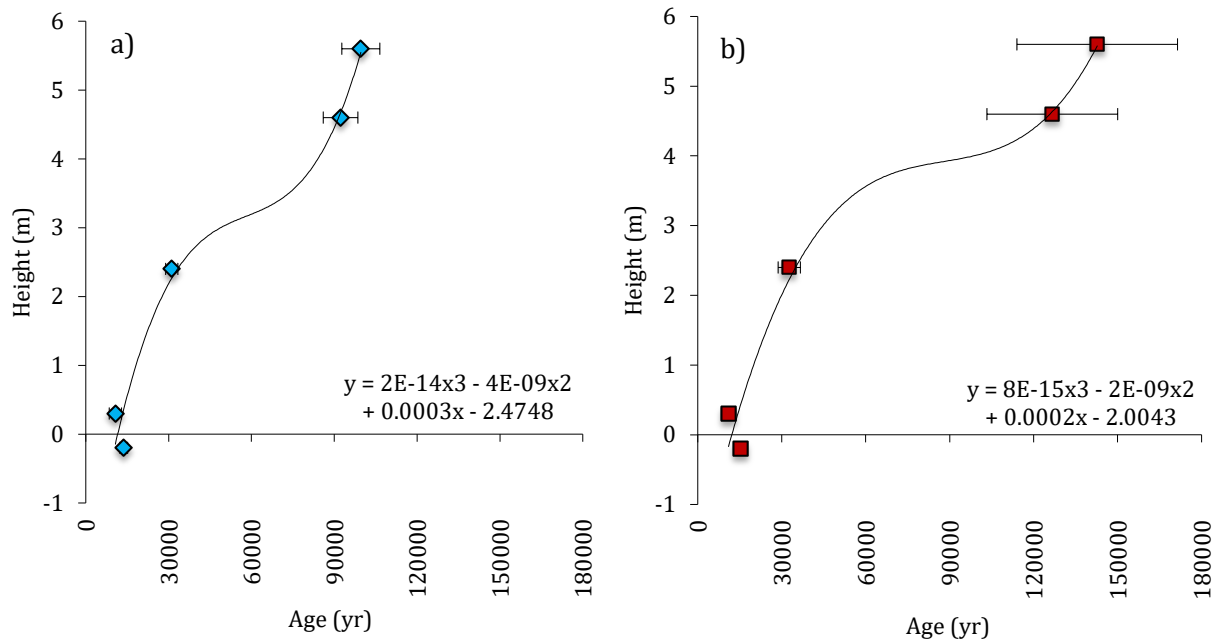
Figure 10. Exposure ages of boulder 2 in correlation to sample heights. Minimal ages (a) in blue and maximum ages (b) in red.

For a more precise surface lowering rate and hence the calculation for soil erosion rates for boulder 2, shorter time steps were chosen and a derivation of the polynomic functions from figure 10 applied. The complete table is attached in the appendix and shows all surface lowering rates (mm/yr) as well soil erosion rates (t/km²/yr) for minimal and maximal rock erosion of 0.0001 cm/yr, and 0.0005 cm/yr, respectively, between 100-140'000 years BP. The results for the surface lowering rates with minimal rock erosion range from 0.02-0.64 mm/yr and for maximal rock erosion from 0.01-0.14 mm/yr.

For minimal rock erosion the derived soil erosion rates range from 14-524 t/km²/yr with its minimum value around 50'000 years and maximum value at 140'000 years. The calculations with maximal rock erosion lead to less soil erosion rates with a range from 6-116 t/km²/yr with lowest rates around 75'000 years. Figure 21 shows the results of the derived soil erosion rate over time in combination with MIS and different climate phases.
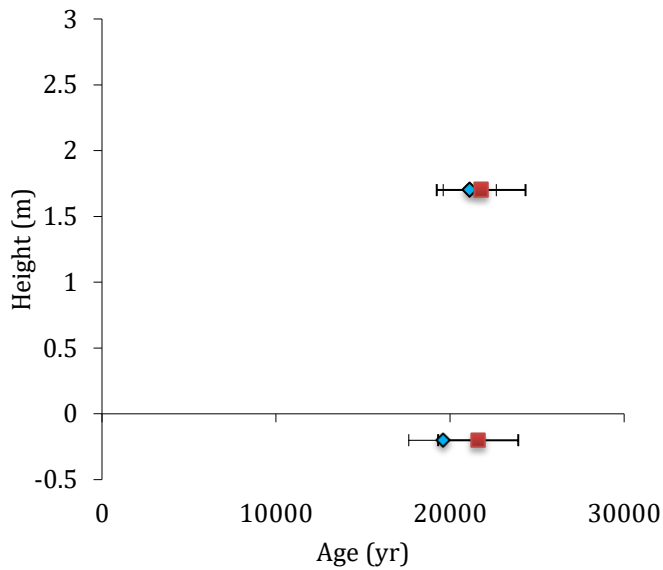
Figure 11. Exposure ages of boulder 3 in correlation to sample heights.
Minimal ages in blue and maximum ages in red.

Bo 3 was only sampled on 3 different levels, where one sample did not get any value in the AMS. Therefore, the results of Bo 3 simply consist of two results (see figure 11 and table 6). The sample under soil surface level, which is not yet exposed has a pre-accumulation of [10]Be from the last 19'600- 21'600 years. On top of the boulder an exposure age of 21'100-21'800 years was calculated. The difference accounts only maximal 2'200 years. This leads to an estimated surface lowering between the samples of 1.255-11.234 mm/year.

Table 6. Surface exposure dating of boulder 3 with minimum and maximum
ages according to CRONUS.

	Bo 3/-20	Bo3/170
Shielding correction	0.612	0.998
[10]Be (atoms/g)	1.67E+05	2.65E+05
Measurement error (%)	5.10%	5.20%
Min. exposure age (yr)	19'614 ± 1986	21'128 ± 1526
Surface lowering (mm/yr)	1.126	
Max. exposure age (yr)	21'614 ± 2301	21'783 ± 2550
Surface lowering (mm/yr)	10.06	

4.2   Relative rock weathering

Average r	225 cm	76 cm	25 cm	10 cm
	38.4	41.7	50.5	40.1
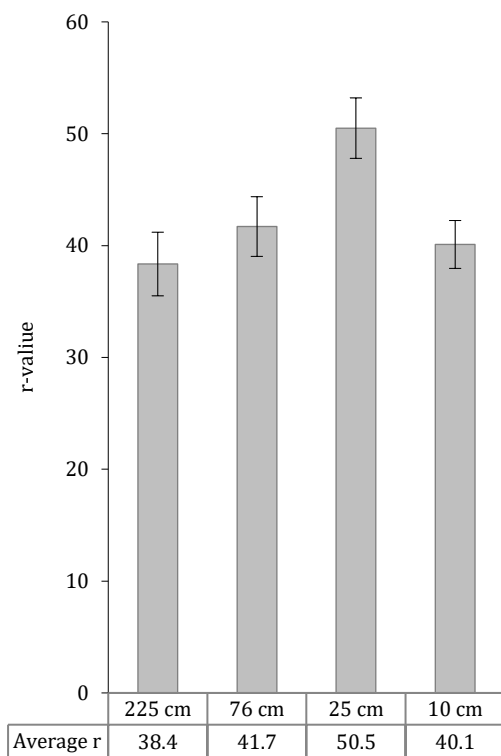
Figure 13. Schmidt-Hammer results for relative rock weathering on boulder 1 at different sampling heights.

Average r	560 cm	460 cm	240 cm	135 cm	30 cm	-20 cm
	39.8	41.1	41.5	41.6	40.4	53.3
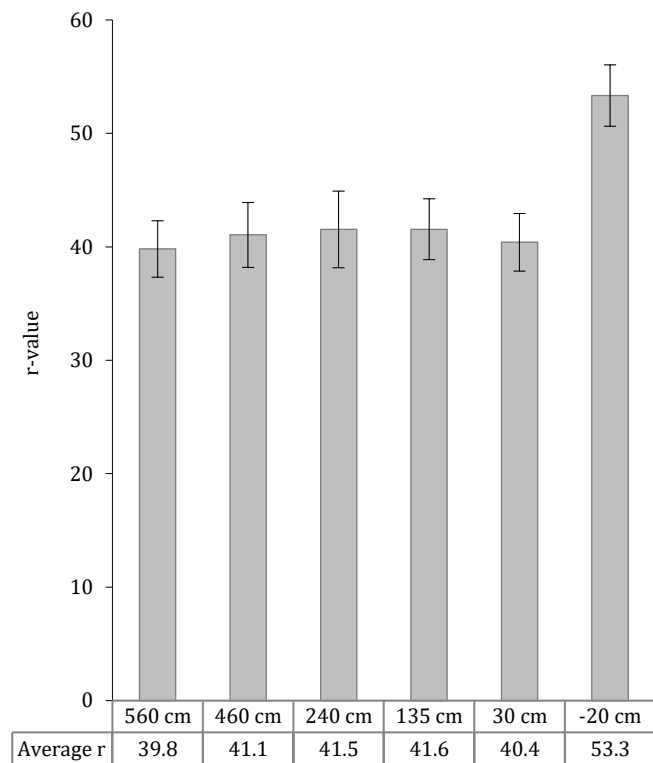
Figure 12. Schmidt-Hammer results for relative rock weathering on boulder 2 at different sampling heights.

Average r	170 cm	120 cm	- 20 cm
	41.2	40.0	47.3
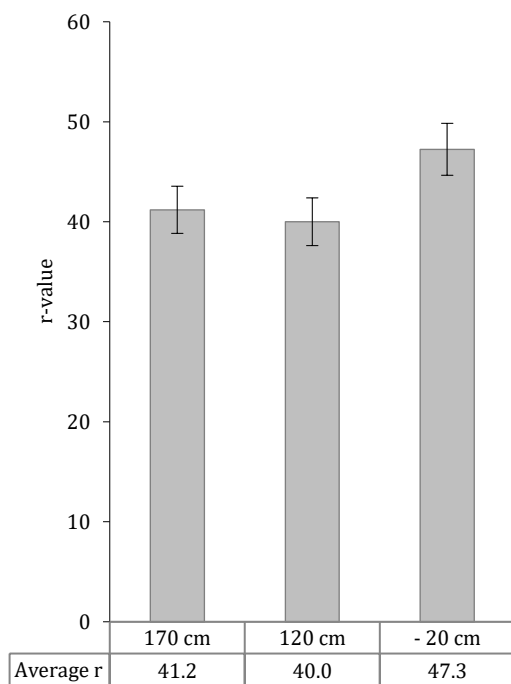
Figure 14. Schmidt-Hammer results for relative rock weathering on boulder 3 at different sampling heights.

The results from the Schmidt-Hammer method, which gives information about the relative rock weathering is shown for all three sampled boulders in figure 12, 13, and 14.

Bo 1 has measured rebound values from 38.4-50.5. The r-values increase towards the soil surface from 38.4 at 225 cm up to 50.5 at 25 cm. Close to the soil surface at 10 cm the value decreases again to 40. Bo 2 shows even r-values for all sampled spots above soil surface. The values range between 39.8- 41.6 with very little varieties between the different profile levels. Only the sample spot under the soil surface has a significant higher r-value with an average of 53.3. The measured values on Bo 3 follow the same pattern like Bo 2. The r-value for -20 cm is noticeable higher than the taken measurements above soil surface, which have a value around 40.

4.3 Stable carbon isotopes

4.3.1 Carbon content

The total carbon C_{tot} content, consisting of C_{org} and C_{inorg}, was measured using a CHN analyzer. Since the soil samples were carbonate free, the total carbon represents therefore the organic carbon content. The C content was also measured while performing the $\delta^{13}C$ analysis. The results are close to those from the CHN analysis with a mean difference of 0.27% C content. Because the CHN analyzer is constructed to measure C content, the results from this measurement are considered in this thesis and listed for each site in table 7, 8, and 9.

Table 7. Carbon content in % on reference site R as a function of profile depth.

Sample site	0-3cm	3-6cm	6-9cm	9-12cm	12-15cm
R1	19.04	6.17	5.10	5.46	5.34
R2	10.82	7.42	6.58	6.01	5.96
R3	12.79	5.95	5.54	5.12	6.80
R4	18.78	6.28	4.75	4.73	4.91
Average C_{tot} R	15.4	6.5	5.5	5.3	5.8
Standard error	1.81	0.29	0.34	0.24	0.36

The C content measured on the reference site is noticeable higher from the content on the investigation sites A and B. In the upper 3 cm the content is highest and varies heavily leading to a mean value of 15.4%. With increasing depth, the C content decreases to mean values from 6.5% to 5.3%. The four replicas show very similar results, especially in the depth profile from 3-15 cm.

Table 8. Carbon content in % on investigation site A as a function of profile depth.

Sample site	0-3cm	3-6cm	6-9cm	9-12cm	12-15cm
A1	7.00	2.55	2.21	1.62	1.92
A2	5.54	1.93	1.65	1.57	1.09
A3	5.10	1.77	1.63	1.76	1.54
A4	7.44	1.95	1.70	1.49	1.59
Average C_{tot} A	6.3	2.0	1.8	1.6	1.5
Standard error	0.49	0.15	0.12	0.05	0.15

On the site A, the carbon content is much lower than on the reference site. The value is like on site R highest in the top soil from 0-3 cm depth with a mean C content of 6.3%. It decreases in the profile to 1.5% in 15 cm depth. The values in the four taken replicas are very consistent without measured outliners.

Table 9. Carbon content in % on investigation site B as a function of profile depth.

Sample site	0-3cm	3-6cm	6-9cm	9-12cm	12-15cm
B1	8.47	2.34	1.72	1.12	1.22
B2	10.44	3.42	1.52	1.46	1.40
B3	4.84	1.94	1.66	1.52	1.51
B4	8.19	2.44	2.34	1.71	1.50
Average Ctot B	8.0	2.5	1.8	1.5	1.4
Standard error	1.58	0.48	0.35	0.31	0.27

Site B shows comparable results to site A. The C content is highest in the top samples from 0- 3 cm depth, but the values vary strongly from 4.8% to 10.4%. With increasing soil depth, the C contents are more consistent between the replicas and a downward trend to a lower C content is measured. The results in the lower top soil from 3-15 cm are equivalent to those measured at site A.

Figure 15 shows the comparison in C_{tot} content of the investigation sites A and B, and the reference site R. The values are highest on the reference site, especially in the top 3 cm of the profile depth. All sites show a decreasing C content with increasing soil depth, in which the C_{tot} decreases at least 5% on the sites A and B and almost 10% on site R.
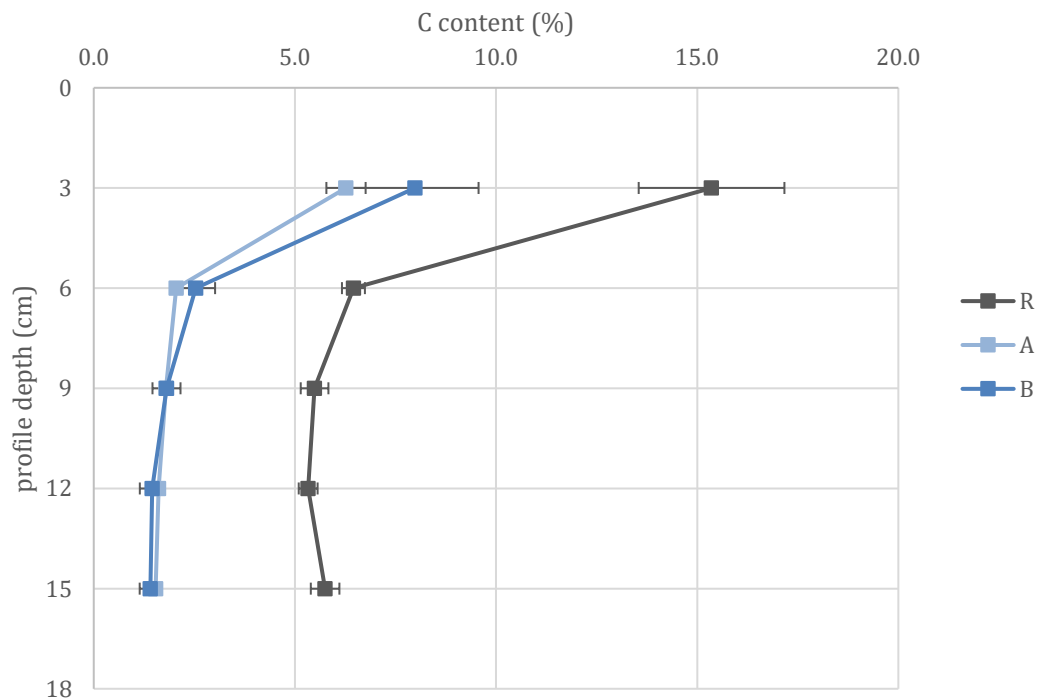
Figure 15. Total C content in a depth profile from 0-15 cm on the investigation sites A, B and reference site R.

4.3.2 Isotope signature

The measured carbon isotope signatures are measured for each profile and used as a qualitative indicator for soil disturbances. The listed results in table 10, 11, and 12 are reported as $\delta^{13}C$ values in ‰.

Site A shows an increasing trend of $\delta^{13}C$ values with increasing depth. Especially in the top 3 cm the value increases over 1.5‰. In depth from 3-9 cm the signature comes to a steady state at around -26.5‰ before it increases again almost 1‰ on a mean value of -25.7‰ at 15 cm soil depth.

Table 10. $\delta^{13}C$ signatures in ‰ of investigation site A as a function of profile depth.

Sample site	0-3cm	3-6cm	6-9cm	9-12cm	12-15cm
A1	-27.96	-26.90	-26.59	-26.30	-26.06
A2	-28.43	-25.75	-26.33	-26.32	-25.65
A3	-27.90	-26.44	-26.33	-25.91	-25.89
A4	-28.19	-26.76	-26.48	-25.86	-25.20
Average $\delta^{13}C$ A	-28.1	-26.5	-26.4	-26.1	-25.7
Standard error	0.105	0.221	0.054	0.108	0.162

The investigation site B shows a similar trend as site A with an increasing $\delta^{13}C$ value in depth. The increase is highest close to the soil surface with 1.4‰ difference in 3 cm depth from -28.1‰ to -26.7‰ mean values. The $\delta^{13}C$ increases further to -25.5‰ at 12 cm, where it comes to a steady state. In general, the trend is more even in depth than site A and shows lower variances within the measurements of the four replicas.

Table 11. $\delta^{13}C$ signatures in ‰ of investigation site B as a function of profile depth.

Sample site	0-3cm	3-6cm	6-9cm	9-12cm	12-15cm
B1	-28.30	-26.70	-25.63	-25.54	-25.33
B2	-28.18	-27.10	-25.86	-25.47	-25.48
B3	-27.76	-26.31	-25.73	-25.53	-25.75
B4	-28.11	-26.67	-25.82	-25.54	-25.25
Average $\delta^{13}C$ B	-28.1	-26.7	-25.8	-25.5	-25.5
Standard error	0.100	0.139	0.045	0.014	0.095

Table 12. δ¹³C signatures in ‰ of reference site R as a function of profile depth.

Sample site	0-3cm	3-6cm	6-9cm	9-12cm	12-15cm
R1	-27.99	-26.80	-26.28	-26.34	-26.37
R2	-27.74	-26.93	-26.74	-26.55	-26.55
R3	-27.89	-26.69	-26.34	-26.33	-26.52
R4	-28.10	-26.85	-25.95	-26.07	-26.60
Average δ¹³C R	-27.9	-26.8	-26.3	-26.3	-26.5
Standard error	0.066	0.043	0.139	0.085	0.043

The reference site shows an increase of $\delta^{13}C$ with soil depth as well. The measurement in the upper 3 cm soil are slightly over -28‰ and increase up to an equilibrium of -26.3‰ in 6- 12 cm depth. In the lowest measured depth at 12-15 cm the isotope signature decreases slightly.

In comparison with site A and B the reference site R shows a higher signature in the upper soil and lower values in depth as illustrated in figure 16. The increase is not as distinct as the values on the investigation sites, on which the increasing $\delta^{13}C$ trend is considerably higher between - 28.1‰ to -25.5‰ in comparison to -27.9‰ to -26.5‰.
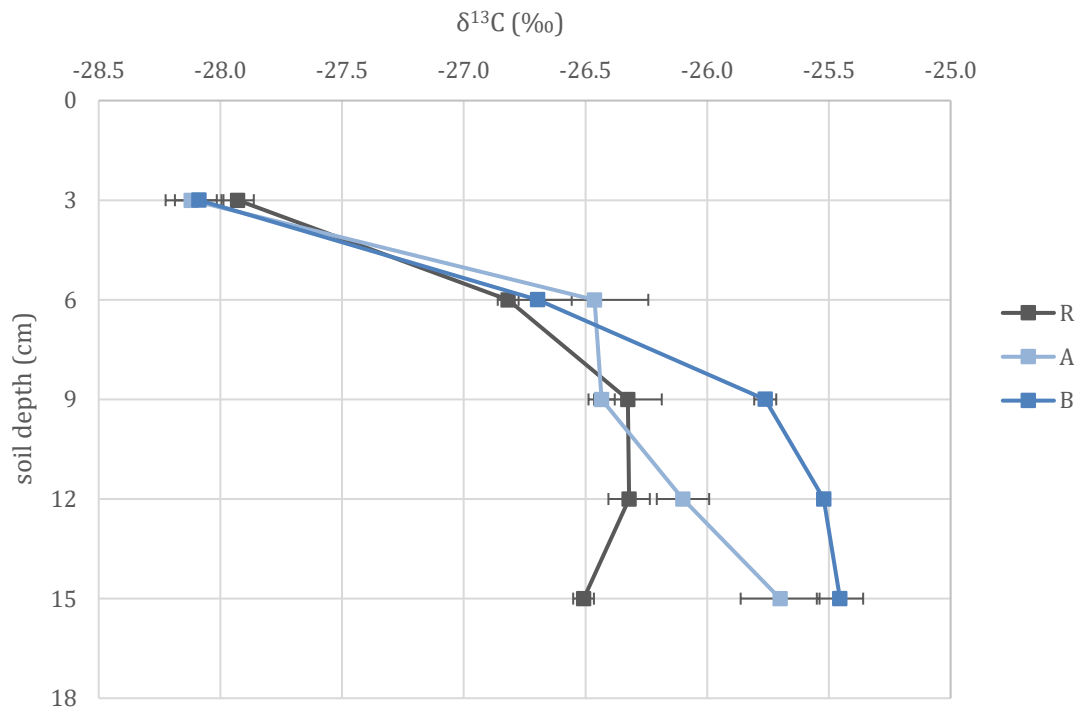
Figure 16. Isotope signatures in the soil profiles with increasing depth.

4.3.3 Correlation

a) Reference site

b) Site A

c) Site B
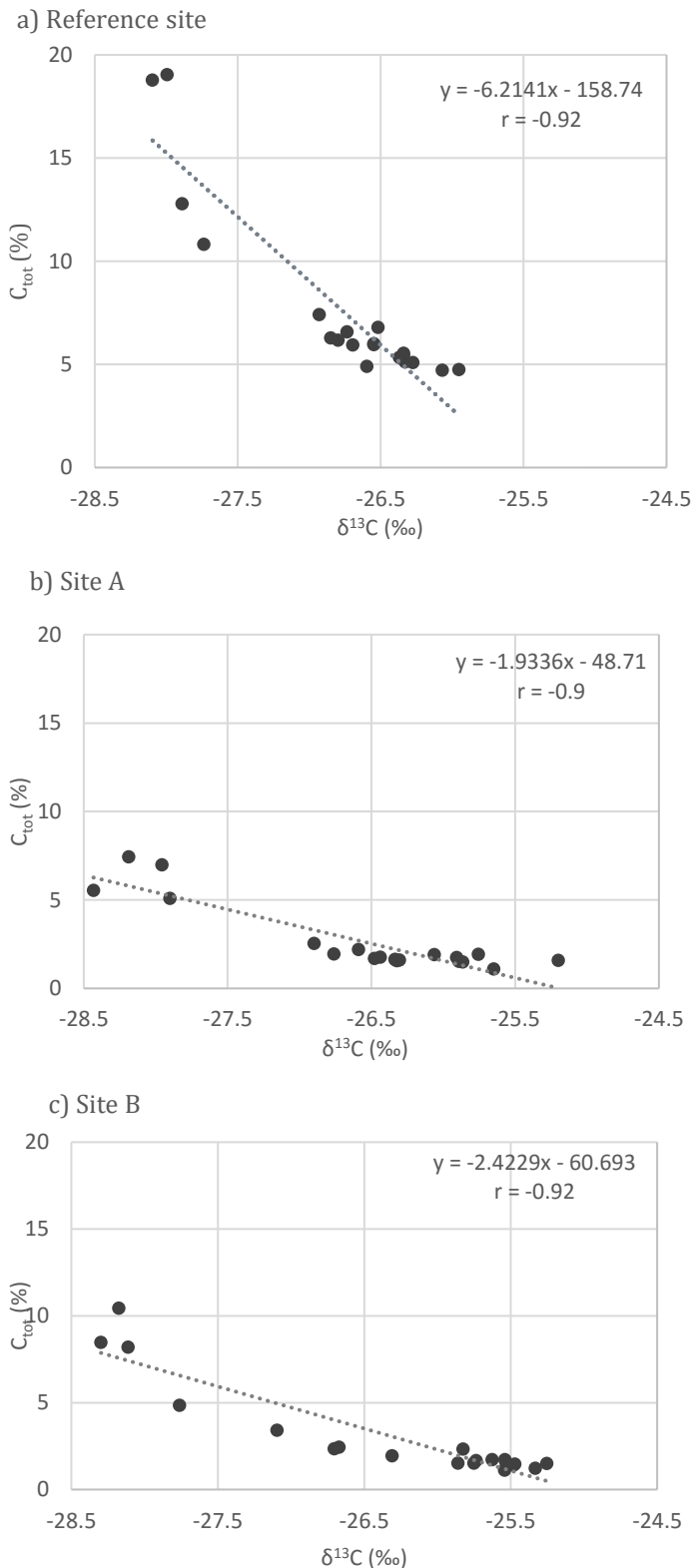
Figure 17. Correlation between carbon content and δ13C values for reference site (a) and investigation sites A (b) and B (c).

The δ13C isotope signatures are measured in the same profile depth like soil carbon content and are therefore comparable to each other. The scattered plot in figure 17 shows the correlation of the two analyzed carbon measurements for the three sites in Sila Massif. 20 measurements were taken at each site and plotted against each other. In general, a very high correlation is detectable with a correlation coefficient r ≥ -0.9. The negative value indicates an indirect correlation between the C content and the isotope signature. Meaning that high C values correlate with more negative δ13C values.

Since C_{tot} is lower on the sites A and B, the trendline for this study sites show a lower slope (m = -2 and -2.5, respectively) compared to site R, with a steep slope (m = -6.2).

4.4   Radionuclide fallout

[239+240]Pu activity was present and therefore detectable in all soil samples. The Pu atom ratios are consistent with those expected from the stratospheric fallout in the Northern Hemisphere of 0.180 ±0.014 (Ketterer 2016, and Kelley et al., 1999).

The results for Pu inventory and soil erosion rates are displayed in table 13, 14, and 15 for each study site and a direct inventory comparison in figure 18.

Table 13. Inventory and soil erosion rate by Pu analysis for reference site R.

Sample site	0-3cm	3-6cm	6-9cm	9-12cm	12-15cm	Inventory (Bq/m^2)	Soil erosion rate (t/km^2/yr)
R1	7.34	13.61	12.26	17.68	13.43	64.33	
R2	9.53	18.31	16.04	18.60	24.23	86.70	
R3	4.19	16.76	14.20	24.87	31.63	91.63	
R4	5.60	10.12	6.06	9.03	13.25	44.06	
Average R	6.66	14.70	12.14	17.54	20.63	71.68	
Standard error	1.00	1.57	1.88	2.82	3.87	9.49	

The reference site shows comparably high Pu inventories between 44 Bq/m^2 and 92 Bq/m^2, leading to an average of 71.68 Bq/m^2. The inventory increases with soil depth from an average value of 6.6 Bq/m^2 to 20.6 Bq/m^2. Since the reference site is to be expected without soil disturbance, the soil erosion rate is set to zero.

Table 14. Inventory and soil erosion rate by Pu analysis for site A.

Sample site	0-3cm	3-6cm	6-9cm	9-12cm	12-15cm	Inventory (Bq/m^2)	Soil erosion rate (t/km^2/yr)
A1	4.54	9.69	8.03	6.54	10.69	39.49	955
A2	2.80	4.97	3.51	5.34	2.71	19.34	1563
A3	3.92	4.12	5.16	8.76	3.93	25.89	1364
A4	4.02	4.14	5.78	8.00	7.82	29.76	1267
Average A	3.82	5.73	5.62	7.16	6.29	28.62	1287
Standard error	0.32	1.16	0.81	0.66	1.58	3.65	110

The inventory of site A and B have significant lower values than the reference site. The average inventories are comparable to each other with 28.62 and 28.19 Bq/m², which results in a loss of 60% to the reference site. Site A and B detect no clear trend with profile depth. The values range from around 3.30 Bq/m² to 8.04 Bq/m² and the inventory accounts approximately one third of the reference site. As figure 18 illustrates the inventories on sites A and B show almost continuous values of 5.5 ± 2 Bq/m².

Table 15. Inventory and soil erosion rate by Pu analysis for site B.

Sample site	0-3cm	3-6cm	6-9cm	9-12cm	12-15cm	Inventory (Bq/m²)	Soil erosion rate (t/km²/yr)
B1	2.82	3.42	7.90	7.10	5.72	26.97	1320
B2	2.53	5.76	6.20	8.25	5.93	28.66	1276
B3	5.01	7.02	5.05	11.12	6.75	34.95	1102
B4	2.82	4.67	2.11	5.69	6.90	22.19	1516
Average B	3.30	5.22	5.31	8.04	6.33	28.19	1304
Standard error	0.50	0.66	1.06	1.00	0.26	2.28	74

The soil erosion rates for the sites A and B are calculated in comparison to the reference site R, which should have no erosion. Site A has slightly lower erosion rates with an average of 1287 t/km²/yr (with a range of 955-1563 t/km²/yr) Site B has in average an erosion of 1304 t/km²/yr (with a range of 1102-1516 t/km²/yr).
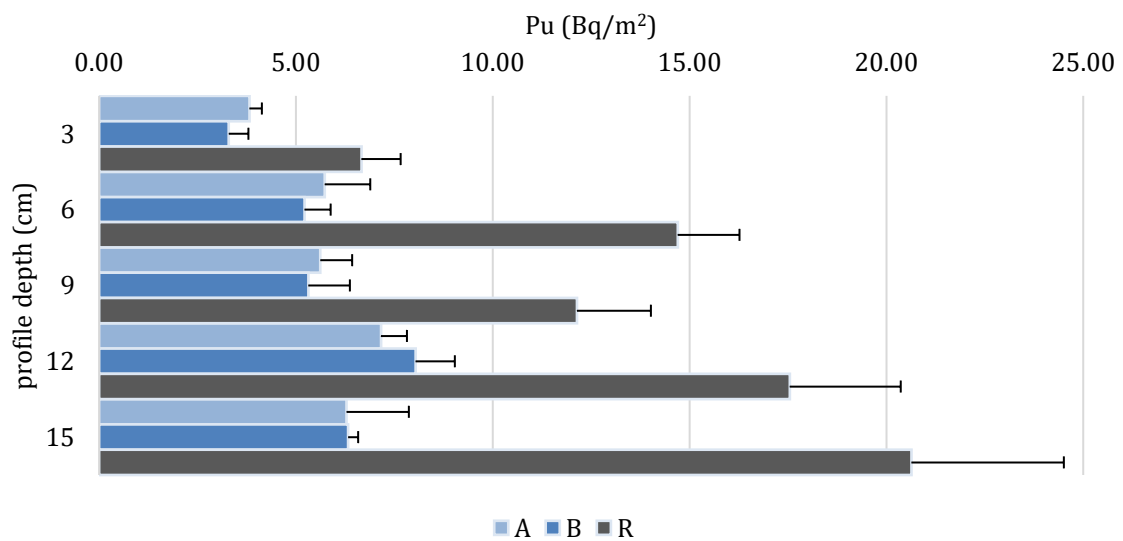
Figure 18. Inventory of Pu in Bq/m² of the investigation sites A and B and reference site.

5 Discussion

5.1 Exposure age

The calculated exposure ages on the three sampled boulders give an approximate time span of their denudation in the past. The hypothesis, that the boulders were exposed from top to bottom and over which period will be discussed in this chapter.

Boulder 1 (Bo 1) has very inconsistent exposure ages along the profile of the rock surface from bottom to the top of the boulder. The sample on top of the boulder turned out to be younger than the sample at the bottom. Supposedly, because this boulder has shifted its position. The exact turnover is difficult to reconstruct, since some samples at different levels above soil surface have the same exposure age. Probably, the boulder is turned upside down. An argument for this hypothesis is the exposure age of the three samples highest at Bo 1. They line up in reverse order of their exposure age ranging from 24'000 years up to maximum 77'000 ± 11'000 years. The samples at 25 cm and 76 cm do not fit in this trend and have probably been exposed before the respective level was reached. The bottom sample at 10 cm height above soil surface with an exposure age of 80'000 years confirms the supposed rotation of Bo 1.

Transferring these results on the timeline in figure 19, Bo 1 was exposed during late Pleistocene. This stage represents the Würmian glaciation in the Alps (MIS 5 – 2), which is equivalent to the Weichselian Stage in NW Europe. It occurred between 115'000 – 11'700 years BP and includes the last glacial maximum (LGM) at around 21'000 years BP, which corresponds to MIS 2 (IPCC, 2013). All calculated exposure ages of Bo 1 are dated within this glacial stage.
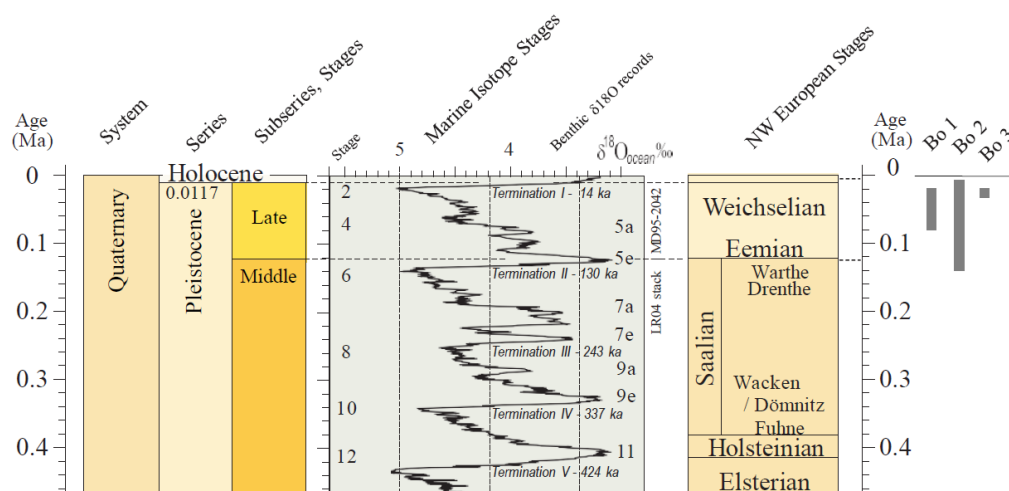
Figure 19. Chronostratigraphical correlation table for Europe modified after international commission on Stratigraphy (ICS, 2016) including exposure ages of Bo 1, Bo 2, and Bo 3.

Boulder 2 (Bo 2) shows a clear increase of age with sample heights. Therefore, it can be assumed, that this boulder has not shifted its position. According to the exposure ages, an exhumation within the last 100'000-140'000 years is expected. The samples are continuously taken between 1-2 m height difference. However, the exposure ages show big time steps especially from sample heights at 240 cm and 460 cm with 60'000-95'000 years in between. The exposure of Bo 2 refers mainly to late Pleistocene and the Holocene as shown in figure 19. The oldest exposed material with an age of 100'000–140'000 years was uncovered during the last interglacial period in Europe, the Eemian stage, which occurred from 115'000- 130'000 years BP (MIS 5e) with warmer and wetter climate conditions. The Eemain interglacial stage was followed by the Würmian glacial stage, where most of Bo 2 was exposed. The youngest denudated material on lowest levels above soil surface have an age of 10'000– 15'000 years and fit therefore in the Holocene Series, which is an interglacial stage. The exposure age with the corresponding sample heights is illustrated in figure 20.

The two samples from boulder 3 (Bo 3) have been dated at 19'600-21'700 ± 2500 years and are exposed in late Pleistocene as well. The exposure age fits very well to the LGM and therefore also MIS 2. Because the ages are close together and even show overlapping uncertainties, a clear trend is not detectable for this boulder. Probably the material on lower level is still exposing and therefore an exhumation during Holocene is plausible. However, it is not possible to tell, if Bo 3 ha shifted over time. Due to the close position to Bo 1, which has probably shifted, Bo 3 might also be influenced by the slightly tilted subsurface.

5.2   Surface lowering and long term erosion rate

The surface lowering rates are calculated for the time steps in between the rock samples. Since these sometime include very big time steps, as discussed in the previous chapter about exposure age, the surface lowering rates give only minimal information about the development of the phases. One can assume that on different phases the surface lowering and erosion rates were influenced especially by climate conditions.

On the one hand, the surface lowering is enhanced by heavy snow masses pushing down the soil surface and exposing the boulders, on the other hand the soil erosion is inhibited in this phase because of a decrease of chemical weathering with lower temperatures, less precipitation and a tundra-like or even slight forest vegetation cover. During wet phases the physical weathering increases because of physical erosion and leaching processes. Therefore, dry and cold phases preserve the soil from erosion, whereas wet and warm phases support erosion.

In general, the calculated surface lowering rates for Bo 1 are very low. The rates are only calculated for the highest taken samples on this boulder, which shows a clear trend. The lowering rate has negative values, meaning there is an accumulation of soil, hence a soil surface uplift. Olivetti et al. (2012) refer to a surface lowering instead, due to a tectonic uplift in this area. Assuming that this boulder is turned over, the calculated surface lowering rate will turn into positive values, confirming the surface lowering, which can also be detected on surrounding boulders in the area shown in figure 4. The surface lowering rate then accounts 0.006-0.06 mm/yr.

For boulder 2, the surface lowering could be calculated between all taken samples and has positive values, confirming the surface lowering in the area. The polynomic trendlines in figure 10 show clear phases with a higher surface lowering, indicated by a steeper function slope and lower surface lowering rates with lower slopes. The rates are in general highest between the longest exposed materials on upper boulder surface levels. As discussed earlier this material might have been exposed in the Eemian interglacial stage, where a higher erosion rate is probable due to warmer and wetter climate conditions. The low surface lowering rates of 0.023 – 0.036 mm/yr between the exposed materials of 32'000–120'000 years confirm the Würmian glacial stage. In the followed time span, between 10'000–32'000 years not only the LGM is included, but also the change to the Holocene at 11'700 years. The assumed low surface lowering rate in the maximum extend period of the cold phase is probably falsified by the impact of the change to the warmer period. Especially in the beginning of a warm phase, more soil disturbances are expected due to more physical and chemical erosion. The calculated lowering rate is an average value of this time span and therefore does not differ between warm and cold phases. The average surface lowering rate of 0.052 – 0.076 mm/a leads to an average soil erosion rate of 42 – 61 t/km^2/yr. Since the boulder was exposed within the last 100'000-140'000 years, the low average erosion rate is influenced by glaciation.

The very close exposure ages on Bo 3 lead to a very high surface lowering rate of at least 1.126 mm/yr, corresponding to 917 t/km^2/yr. This value is most likely too high, taking into account that no other value is available to support it. Even though one cannot confirm the high erosion rate, it is possible that during the last 20'000 years an increase in erosion has taken place due to a change in climate conditions from a cold to a warm phase. Especially the transition period is known to have an increased soil erosion, since ice and snow melt lead to more fluvial erosion and chemical erosion processes are supported by higher temperatures.

Since big sampling steps on the boulder surface result in big time steps, the surface lowering rates represent average values in between the sampling heights. For more precise values, more differentiated rates for Bo 2 were calculated using polynomic functions. The precise

rates are given in the appendix table 5 for a time span of 140'000 years. It becomes clear, that during the Holocene, comparably high surface lowering rates with values of 0.17 – 0.11 mm/yr are calculated. Extrapolated to soil erosion rates this results in values from 90 – 141 t/km²/yr. In the late Pleistocene, the erosion rates decrease rapidly to 14 t/km²/yr for minimal rock erosion and to 5 t/km²/yr for maximal rock erosion. Resulting in surface lowering rates between 0.05 – 0.01 mm/yr, which is very low and indicates almost a standstill during this last glacial phase. The lowest calculated erosion rate is between 25'000 – 70'000 years for minimal rock erosion and between 30'000 – 120'000 years for maximal rock erosion (see figure 21). The average soil erosion rates between the samples along the boulders' surface are displayed in figure 20 with its respective sample heights and surface exposure age.
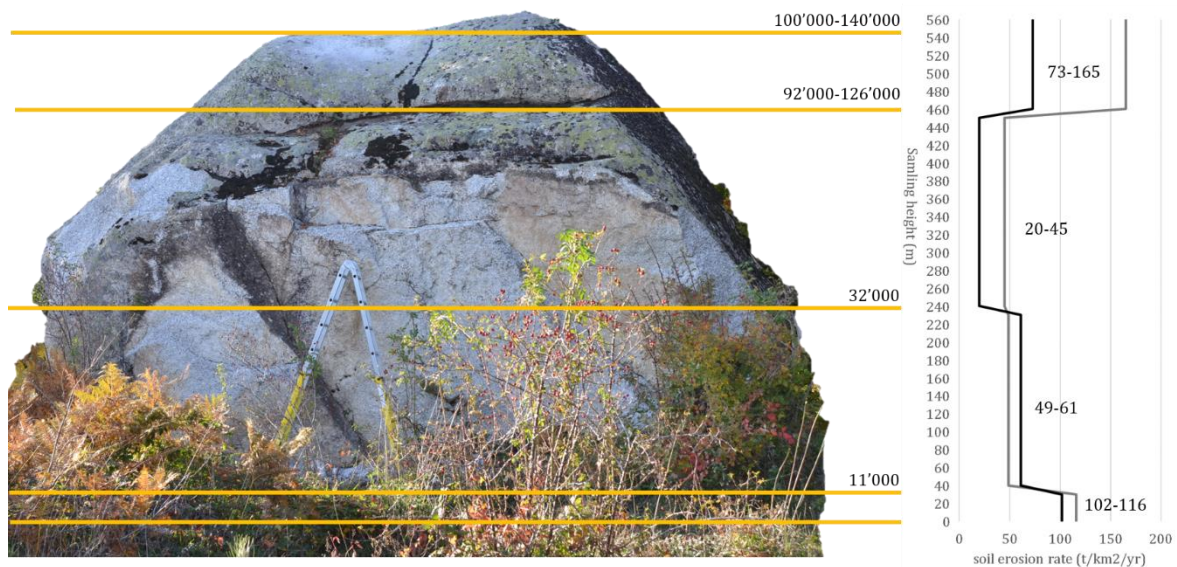
Figure 20. Exposure ages (years BP) and soil erosion rates (t/km²/yr) along the surface level of boulder 2.
(Black line for soil erosion rate calculated with maximum rock erosion, grey line with minimum rock erosion)

It is clearly visible that the top of the boulder was exposed over a short time period with high soil erosion rates. The middle part of bo 2 was denudated very slowly with average soil erosion rates of maximal 45-61 t/km²/yr. The bottom part of this boulder was exposed in the Holocene over the last 11'000 years with again high average rates.

As discussed above a minimum erosion is set in the late Pleistocene before the LGM, which occurred approximately at 21'000 years BP (IPCC, 2013). According to Hughes et al. (2006), a maximum glaciation accompanied by very cold climate conditions took place in Italy before the LGM in the Alpes. The derived low soil erosion rates support this earlier distinct glacial phase in the Sila Mountains. Since the study area is located on an elevation of 1572 m

a.s.l. it is possible that this area was partially covered by the glaciers, because other Italian regions register glaciers extensions to an altitude of 1500 m a.s.l. (Huges et al., 2006, and Messerli, 1967). There is an increase of soil erosion towards 100'000 years (minimal rock weathering) and 125'000 years (maximal rock weathering) as shown in figure 21.
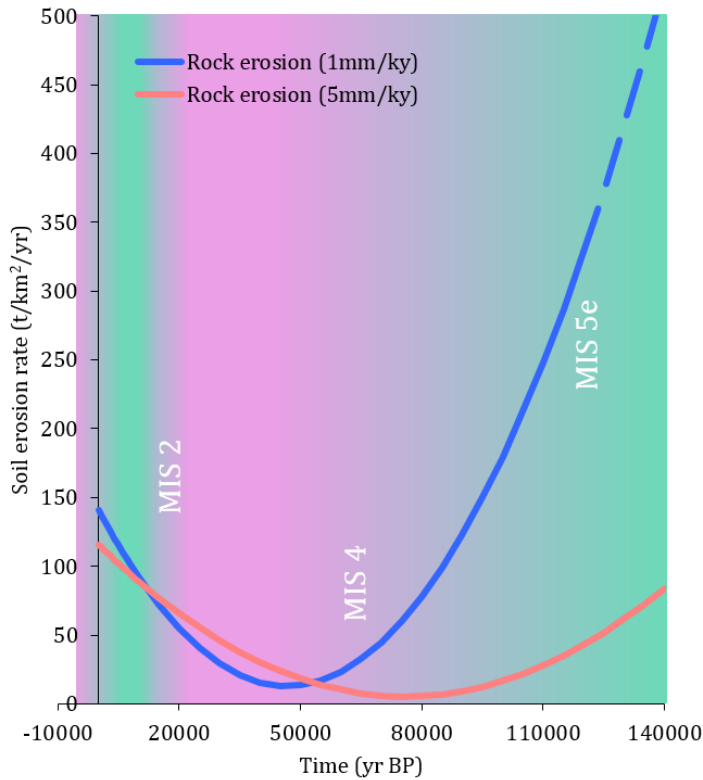
Figure 21. Soil erosion rate in time of boulder 2. Turquoise indicates wet climate conditions, lilac dry ones.

The blue derived rates in figure 21 show a fast increase of 100 – 300 t/km²/yr in the Eemian interglacial stage with an illustrated dashed extrapolation up to 500 t/km²/yr at 140'000 years. The red derived soil erosion also increases in this time span. The Eemian interglacial stage is linked to the MIS 5e with warm climate conditions, which enhance the erosion process and confirm the derived erosion rates.

Messerli (1967) investigated the Mediterranean area during the Würmian glacial stage, in which different conditions lead to uneven glacial extensions. With interpretations from glacial landscapes he suggested, that the area was formed by wet and cold conditions during the early-to-maximum Würmian stage with more precipitation and glacier melt during summer compared to the dry and cold late Würmian stage.

In figure 21, the phases with high precipitation, equal to wet phases, are illustrated in turquoise, whereas the late Würmian glacial period, which is poor in precipitation is colored in lilac to point out dry phases.

Overall the calculated soil erosion rates match the glacial and interglacial stages of the Holocene and late Pleistocene, but for a more detailed analysis about erosional phases more samples need to be taken on smaller sampling steps along the boulders surface to investigate smaller time steps. Furthermore, a bigger variety of boulders could help to crosscheck the exposure ages and soil erosion rates to support the hypothesis of denudation phases.

5.3   Relative rock weathering

The relative rock weathering measured with the Schmidt-Hammer should indicate a longer exposure time on top of the boulders with lower r-values than at lower surface levels. The results show very consistent rebound values around 40 for all sample spots on the three boulders.

Bo 1 shows a slight increase with sampling height, which would confirm the longer exposed, more weathered material. However, due to the assumption that this boulder has shifted its position, these values are conflicting with this theory. Another reason for higher values is the measuring technique using the device. The access to the sampling spots, especially at 25 cm, was difficult and the positioning of the Schmidt-Hammer not optimal. This might influence the measurements and therefore the rock weathering interpretation. If the sampling spot at 25 cm is considered an outlier, the r- values are around 40 without an increasing or decreasing trend. Compared to Bo 2 and 3, which have similar values, it leads to the conclusion that these boulders have almost no rock weathering. Although it is possible, that the outer layer of the rock has already weathered away and the exposed inner layer is stable. Based on this conclusion, a low rock erosion rate of 0.0001 cm/yr is more probable than the high rock erosion rate of 0.0005 cm/yr. Therefore, the calculated minimum results of exposure ages and long-term erosion rates are considered to be realistic.

5.4 $^{239+240}$Pu inventory

As described in the chapter radionuclide fallout, the Pu is detected through the whole profile depth. The differential results from site R to sites A and B confirm that the investigation sites are somehow influenced by soil disturbances.

The research of Zollinger et al. (2015) and Alewell et al. (2014) shows a decrease in $^{239+240}$Pu with soil depth due to low migration rates of the attached isotopes to SOM. This distribution is typical for undisturbed soils but also appears on disturbed soils with less distinctive values. The trend of the inventory from Zollinger et at. (2015) tends to decrease rapidly in depth to minimal values of 1 Bq/m². The results from the Sila soil however show a more even distribution of Pu as a consequence of bioturbation by animals. Even a clear increase of Pu with depth is detectable on the reference site. For these investigation sites (A and B), an almost constant Pu amount is measured. Through visual investigations of the near surface area, several vole and mole wholes were discovered. These animals most likely turned over the soil layers repeatedly. This process leads to a more homogeneous distribution of Pu in soil depth. An argument against this turnover is the distribution of C_{org}, discussed in chapter 4.3.1 Carbon content on page 32, which changes with soil depth as expected and shows no big influence of animal disturbance.

The maximum inventory is measured on the reference site with 71.68 ± 9.5 Bq/m², which is a little lower than the reference inventory in the Swiss Alps with values around 80-90 Bq/m². According to Zollinger et al. (2015), a range of 50-100 Bq/m² is the expected inventory for the northern hemisphere. Soil erosion lead to an inventory reduction because upper soil layers with the attached $^{239+240}$Pu are transported away. The reduction accounts approximately 32% in the Swiss Alps, investigated by Alewell et al. (2014). In the Sila soil, the inventory loss is especially high with approximately 60%. Due to a more even distribution in depth, the inventory reduction is not only detected in the upper soil layer as observed by the above-mentioned researches, but throughout the whole soil profile. The inventory in depth of 6-15 cm is comparable with the one measured by Zollinger et al. (2015) with low values. Another explanation for the low inventory of the upper layer is a complete erosion of the upper part of the top soil, in which most $^{239+240}$Pu would have been redistributed. Although, this does not explain the increase and inverse distribution of the Pu on the reference site. Not included in the results is the amount of Pu, which was possibly taken up by plants. Roots or plant surfaces can absorb radionuclides and release them when they die and decompose (Zollinger et al., 2015).

5.5   Short term soil erosion rate

The reduction of 60% inventory on the investigation sites A and B correspond to average erosion rates of 1287 t/km²/yr and 1304 t/km²/yr. Compared to Alewell et al. (2014) and Zollinger et al. (2015) these calculated erosion rates are very high. In Switzerland, an average erosion rate of 450-830 t/km²/yr was determined for two alpine valleys and even less for sites close to permafrost with values around 60 t/km²/yr. The high erosion rate in the Sila massif can be explained by a more intensive land use before converting this part of Italy into the Sila National Park. During this time probably also heavy machinery might have been used in agriculture and therefore more surface runoff by rill erosion was the consequence. Nowadays the only apparent land use in this area were extensive grazing horses. Even though the taken samples were collected at visually undisturbed sites with no signs of horse paths or heavy surface runoff, the effect of agriculture until the beginning of the 21th century is reflected in the high erosion rate results. A close look on figure 5 supports the soil disturbances by cultivating the plateau. On the picture one can recognize soil compaction marks from previous access lanes.
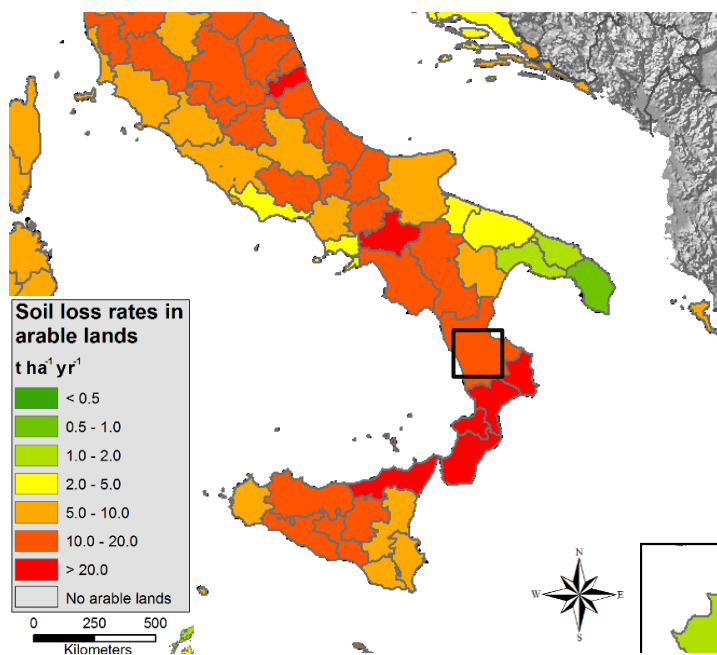
Figure 22. Soil loss rates in Italy modified after Eurostat (2015). The region of Calabria is framed.

The erosion rate guideline value of 2 t/ha/yr given in the regulation of pollution for soils (germ. "Verordnung über die Belastung des Bodens", VBBo, 1998) in Switzerland, corresponds to 200 t/km²/yr. This value would be clearly exceeded by the calculated soil erosion rates in the Sila mountains. This value is a guideline for the tolerable amount of soil erosion on agricultural land in Switzerland. Since meadowland for grazing livestock is a form of agriculture as well, the investigation area would fall into this category.

Statistical analysis by the European Commission classified the soil erosion risk of the Mediterranean region in Italy as moderate high to very high, whereas Calabria has a soil loss rate of 1000-2000 t/km²/yr for arable lands (Eurostat, 2015) as shown in figure 22.

5.6   Comparison of erosion rates

The discussed short-term erosion rate is based on the time period from 1963 until now, because of the global dispersion of Pu through nuclear weapon testing. Long-term erosion rates with [10]Be measurements can be applied for periods over millennia and therefore also include glacial and interglacial phases in Europe.

Table 16 shows a comparison of the long-term to short-term erosion phases, and literature values from the same area. The short-term erosion rates are considerably higher than the long-term erosion rates, because the values of Bo 1 and Bo 2 include cold phases during the late Pleistocene, which lower the average erosion rate. In the Holocene, the erosion rates increase, but still do not catch up with the high short-term erosion rates. The average soil erosion rate for Bo 1 the mean value of the two calculated erosion rates listed in table 4. For Bo 2 an average value of the derived soil erosion rate (see appendix table 5) is taken for the comparison. Bo 3 is left out in the comparison, since only two values were provided, which is not enough information to calculate a reasonable average erosion rate. The comparison between long- and short-term rates highlight, that a distinct increase in erosion has taken place in the last millennia. Mid-term erosion rates over the last centuries would herby give valuable information about the change and development of this strong increase.

Compared with erosion rates derived from river catchments from Olivetti et al. (2012) show that the short-term erosion rates fit into the same range. In this literature, the erosion rates were analyzed in river sediments, with deposited accumulated material. Since Olivetti et al. (2012) calculated the erosion rate for rock material, the values had to be converted into soil erosion rates before comparing them to the results presented in chapter 4. The soil erosion rates for Site A and B match to similar erosion rates between 832-1690 $t/km^2/yr$ from the river catchments. These erosion rates were mainly observed for fluvial valleys in the Sila mountains, where the sediment catchments were already accumulated by various side streams. Olivetti et al. (2012) also investigated upland regions, which should fit better to the surrounding sampling conditions. The results however are five times lower than the erosion rates in the upland plateau of the sites A and B. In conclusion, short-term erosion rates match values from literature whereas long-term erosion does not. Long-term erosion rates from boulder samples have lower values than the ones from river catchments. A possible explanation could be that erosion rates through river catchments are influenced by landslides.

Olivetti et al. (2012) concluded that the strong and unsteady uplift is no yet counterbalanced by erosion, which can be confirmed by the calculated erosion rates of this study.

Table 16. Comparison of soil erosion rates from Sila Upland plateaus with converted literature values from river catchments by Olivetti et al. (2012).

Sila Upland values Sample name	t/km²/yr	Literature values sample name	t/km²/yr
A1	955	Cino	260
A2	1563	Trionto 1b	338
A3	1364	Trionto 3 (Laurenzana)	650
A4	1267	Trionto 4 (Laurenzana)	676
average A	*1287*	Trionto 5 (Ortiano)	1638
		Trionto 6	1482
B1	1320	Trionto 7 (no name trib)	2392
B2	1276	Trionto 8	494
B3	1102	Lese 1	1144
B4	1516	Lese 3	312
average B	*1304*	Lese 5	832
		Lese 6 (Lese Trib2)	936
Bo 1 (min. rock erosion)	28	Tacina	260
Bo 1 (max. rock erosion)	24	Crocchio 1	494
		Crocchio 2	546
Bo 2 (min. rock erosion)	104	Simeri 1	988
Bo 2 (max. rock erosion)	53	Simeri 3	2132
		Simeri Trib	208
		Forestale 1	1690
		Alli 1	234
		Alli 2	1430

5.7   Qualitative soil erosion

Research on stable carbon isotopes as a tracer for soil erosion was done e.g. by Zollinger et al. (2015), Guillaume et al. (2015), Meusburger et al. (2013), and Schaub et al. (2009). In their research, they describe influences of decomposition and erosion on the carbon distribution within soil profiles. Therefore, they compared isotope signatures and C content of disturbed sites to reference sites. The results in the Sila Massif also show differences between the investigation sites A and B, and the reference site R. These are to be discussed and compared with the previously done, above-mentioned research.

Oxic soils are expected to have decomposition processes, in which a kinetic fractionation should be detectable. This occurs because the reaction rates are slower for heavy isotopes

like ^{13}C, than for lighter ones like ^{12}C and leads to an enriched ^{13}C soil (Schaub et al., 2009, and Guillaume, et al., 2015). In the research of Schaub et al. (2009) they describe the reference site as wetland with anaerobic conditions, where no erosion and decomposition is taking place with no significant change of δ^{13}C in depth. Since the entire site in the Sila Massif contains oxic soils, decomposition is assumed which leads to an increase of δ^{13}C with depth. This can be confirmed by the results listed in chapter 4.3.2 Isotope signature on page 34-35. All profiles show an increase of δ^{13}C, whereas the sample sites A and B show a larger increase towards less negative values (approx. 2.5‰) than site R (approx. 1.5‰). This enrichment of ^{13}C can only be observed in the upper horizons of approximately 0-20 cm additionally the effect decreases with soil depth (Guillaume et al., 2015). To the depth increase of δ^{13}C a parallel decrease of C content is found for all profiles. This results from the decomposition of organic material especially in the upper soil part.

Guillaume et al. (2015) points out, that erosion has only an indirect impact on the δ^{13}C value, because soil particles are mechanically transported without considering whether they are light isotopes like ^{12}C or heavy isotopes like [13]C. This means that the erosion process has no influence on the ratio of ^{12}C and [13]C. Nevertheless, the δ^{13}C depth distribution in the profile shifts towards the soil surface, because of the loss of the upper layer (Guillaume et al., 2015). The δ^{13}C results in southern Italy confirm this horizontal shift, by comparing the same isotope signatures at different sampling depths. Especially the values of site A at depth of 3-6 cm and 6-9 cm match the values of site R on the depth of 6-9 cm and 9-12 cm, respectively. The results of sites A and B tend also to less negative δ^{13}C values. This can be interpreted as higher decomposition rates compared to site R. This mixing effect of erosion and decomposition processes is investigated by Guillaume et al. (2015) illustrating the horizontal and vertical shifts in figure 23.
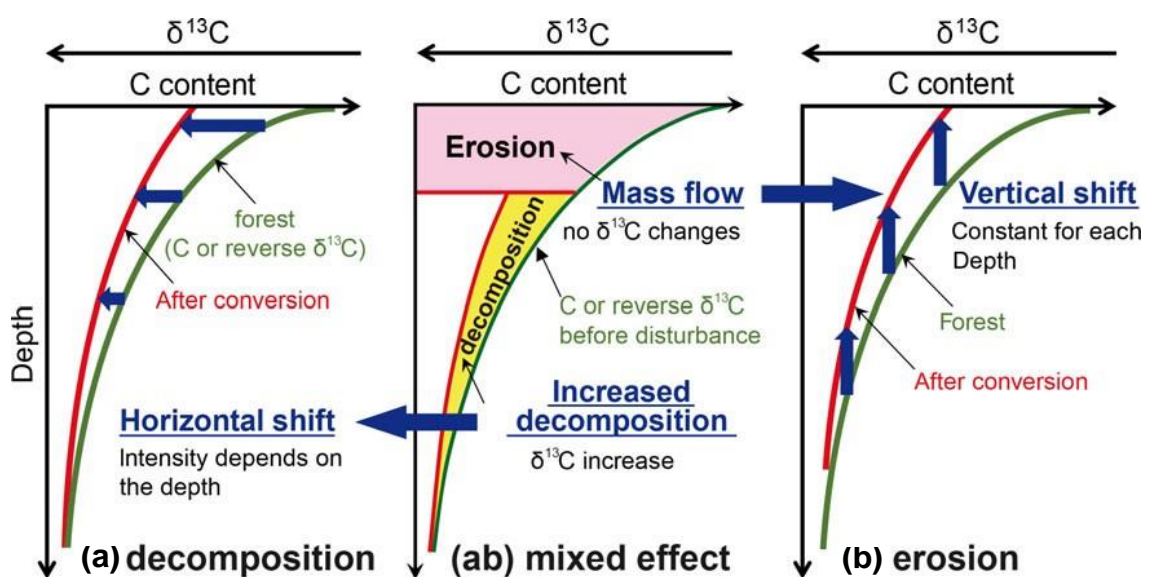
Figure 23. Impact of erosion and decomposition processes on C content and δ^{13}C distribution in soil profiles using the example of forest conversion by Guillaume, et al. (2015).

In contrast to $\delta^{13}C$, erosion has a direct impact on the C content of the soil. During erosion, soil is removed, where SOC is the first to go into suspension in form of small particles, which may lead to leaching of organic carbon (Meusburger et al., 2013). All Sila soil samples show a decrease of 60% C content within the first 6 cm profile depth, regardless of the site. Especially the profiles at site A and B confirm the loss of carbon, because the C content accounts approximately one third of the measured content at site R. The highest measured C content in the profiles at the sites A and B have values around 5-10%, whereas the highest values at the reference site are 10-20%. This lower content of organic carbon on the investigation area can be interpreted by soil loss, and therefore loss of organic carbon.

It is noticeable, that the results on site R within 3-6 cm depth match the values of site A and B within 0-3 cm depth. One explanation for these overlapping values at different depths could be the total erosion of the upper 3 cm on the investigation sites. This means that the upper soil with higher C content is removed and the profile of site A and B start directly with lower soil layers. Based on this hypothesis the values are each displaced by 3 cm in comparison to site R. A problem with this theory is the fact, that the organic C is not removed continuously over the entire profile, but only over the first 3 cm. For site A and B the values decrease with depth until about 6-15 cm soil depth. So does the reference site, but with a higher C_{tot} content. Therefore, the hypothesis of a total erosion of the upper layer cannot be completely confirmed. A vertical shift towards a lower C_{tot} content at the sites A and B is more likely. This shift confirms the C loss with suspension or a higher decomposition rate of organic material.

Schaub et al. (2009) and Meusburger et al. (2013) conclude, that isotopic fractionation accompanies the decomposition of SOC, which results in a strong correlation between C content and $\delta^{13}C$ isotope signature for non-erosive sites. On erosive sites, a weak correlation was observed in their research. Weak correlations are described as a result of the low decomposition rates of organic matter, which may appear under anaerobic conditions. Hence, the correlation reflects the prevailing metabolism during soil formation (Schaub et al., 2009).

The Sila soil however shows very strong correlations on all sampled sites. The difference in correlation between erosion site and control site is not detectable, since the correlation coefficient r varies between -0.90 and -0.92. This would lead to the assumption that the Sila soil samples have a good oxic soil formation with soil organic carbon decomposition. Based on correlation coefficients of Schaub et al. (2009) of r < - 0.8 for erosive and r > -0.8 for non-erosive sites in alpine areas, one could assume, that there is no erosion found in the area of the Sila Massif.

A noticeable difference between the reference site and the investigation sites is, that correlation shows a lower slope of the linear trendline. There is clearly a steeper slope on the reference site, than on the sites A and B, which results in significantly lower C content in the investigation sites, but similar isotope signatures. The results of Schaub et al. (2009) also show steeper slopes of trendlines for non-erosive soils and low slopes for erosion sites. This method is a qualitative indicator for soil disturbances and not suitable for quantitative information about soil erosion rates (Meusburger et al., 2013). For this reason, one can conclude, that there is a difference detectable based on carbon measurements even though they are not as clearly statistical proven.

6 Conclusion

An approximate exposure time of boulders in the upland plateau of the Sila Massif could be set with SED using [10]Be. The results of boulder 2 confirmed the hypothesis of the boulders denudation from top to bottom. The longest exposed material was found in 5.6 m above soil surface and the youngest material on 0.3 m above ground. This boulder exposed over a time span of 100'000-140'000 years, which includes different climatic conditions. Due to a probable shift of boulder 1 and not enough results of boulder 3, the denudation history of boulder 2 could not be compared to other samples.

Different phases in soil development over time could be detected with the exposure age and derived long-term erosion rates. The upland plateau of the Sila Massif experienced regressive phases with more erosion during the Eemian interglacial stage and the Holocene, and less erosion during the Würmian glacial stage. The calculated long-term erosion rates showed a correlation between low rates and not only cold, but also dry phases. High rates could be assigned with to warm and wet conditions. The calculated erosion rates show minimum values before the LGM at 21'000 years, which suggest a possible earlier glacial maximum in the Sila mountains than in the Alps.

To conclude, the denudation could be related to different climates, but not to tectonic phases. The region of the Sila Massif in Calabria had a strong uplift approximately 400'000 years BP. The longest exposed material reaches a maximal exposure age of 140'000 years BP and is therefore denudated after the tectonic uplift phase in the area.

The short-term soil erosion derived from Pu distribution in the area is much higher than the long-term erosion. Compared to the soil erosion rate of boulder 2, the rate is 25 times higher, and in comparison to boulder 1, the erosion rate is 50 times higher. By converting the inventory loss of Pu into soil redistribution rates, the soil erosion could be registered. The investigation sites A and B have a loss of 60% compared to the reference site, which is twice as much as erosive sites in the Swiss Alps. However, the soil erosion rates are comparable with values from previous research about in the same area in Italy. These values support the reliability of the high calculated short-term erosion rates. The presence of digging animals like voles and moles lead to bioturbation of the upper soil profile and distributed the Pu more evenly in soil depth. Therefore, no decreasing trend is detectable on the Sila upland sites as expected.

The C_{tot} and $\delta^{13}C$ however showed a differentiated distribution with profile depth. The investigation sites show half the amount of C_{tot} in comparison to the reference site, which leads to the conclusion that the upper soil layer has been removed by erosion. The isotope signatures are shifted in vertical direction towards less negative $\delta^{13}C$ values on the

investigation sites, and in horizontal direction towards the soil surface level. This combination in both directions indicate mixed effects of erosion and decomposition in the Sila soil. These findings support previously done research that stable carbon isotopes are a qualitative indicator for soil erosion and furthermore confirm the short-term erosion identified by radionuclide analysis in this study.

A reconstruction of the soil formation in the upland Sila plateau in Calabria was achieved over the last hundred thousand years by analyzing the exposure ages of boulders, the long- as well as the short-term soil erosion rates. Over the entire time span a soil regression was detected with its minimum soil erosion rate during the last cold phase and its peak of soil erosion in recent decades.

Acknowledgement

I would like to thank several people, who helped me complete this master thesis.

First of all, my thanks to Prof. Dr. Markus Egli for supervising me and this project with big enthusiasms and commitment. He helped me understanding the context of this work with associated research topics and supported me with calculations, tools, good inputs and discussions, and accompanied me to the field.

I would like to thank Dr. Fabio Scarciglia for his local support in Calabria, where he organized the approval for sampling in the National Park and guided us through the Sila Massif. He supported me with field work, interesting discussions, and literature choices.

Many thanks to Dr. Dagmar Brandovà, who supported me through the entire master thesis. She took a lot of responsibility for my work in the laboratory and helped me not only with sample preparations and lab work, but also with very good advices and moral support. I also would like to thank Max Boxleitner for helping me with sample preparations and assistance in the laboratory, and Sandra Röthlisberger and Ivan Woodhatch for their help with laboratory facilities.

My thanks also to Christine Alewell and her team from the University of Basel, and Michael Ketterer and his team from the Metropolitan State University of Denver, Colorado, who supported this thesis by providing the measurements of the stable carbon isotopes and the radionuclides in their laboratories.

I deeply want to thank my correctors for taking their time to look over my drafts, results, and layout. Knowing that the topic of this thesis is very specific, my gratitude for the time-consuming support with discussions, inputs, and constructive criticism. Additionally, thanks to my friends and family, who encouraged me during the last year. Their support was not necessarily topic related, but even more important they helped me with good conversations and feedback.

In the very end I would like to express my greatest thanks to my parents for supporting me through all my time at University and enable me my academic achievements. They were always on hand with help and advice and supported me with my decisions.

References

Alewell, Christine, et al. 2014. Sustability of 239+240Pu and 137Cs as tracers for soil erosion assessment in mountain grasslands. *Chemosphere 103.* 2014, pp. 274-280.

Balco, Greg, et al. 2008. A complete and easily accessible means of calculating surface exposure ages and erosion rates from 10Be and 26AL measurements. *Quaternary Geochronology 3.* 2008, pp. 174-195.

Christel, Marcus. 2016. *Cover letter 10Be results of July 2016 run.* ETH, Zürich : s.n., 2016.

Colacino, M., Conte, M. and Piervitali, E. 1997. Elementi di climatoloigia della Calabria. [book auth.] Guerrini A. *Collana Progetto Strategico "Clima, ambiente e territrio nel Mezzogiorno".* Roma : CNR-IFA (Istituto di Fisica dell'Atmosfera, 1997, p. 218 pp.

Cosmogenic Nuclide Lab, University of Washington. 2016. CRONUS earth. Cosmic-Ray Produced Nuclide Systematics on Earth Project. [Online] 2016. http://hess.ess.washington.edu/math/al_be_v23/al_be_multiple_v23.php.

Egli, Markus and Scarciglia, Fabio. 2015. Proposal of Project Beryllium: Boulder Exhumation Rates (over 10^5 Years) in Low-gradient Landscapes in an Upland Mediterranean Area. 2015.

Egli, Markus, et al. 2010. 10Be inventories in Alpine soils and their potential for dating land surfaces. *Geomorphology 119.* 2010, pp. 62-73.

Egli, Markus, et al. 2013. *Geochronology laboratory mehtods.* Departement of Geography, University of Zürich. Zürich : s.n., 2013. Lab Script.

Ente Parco Nationale della Sila. 2016. Parco Nationale della Sila. [Online] 2016. http://www.parcosila.it/it.

Eurostat. 2015. Agri-environmental indicator - soil erosion. [Online] 2015. [Cited: 9. 10, 2016.] http://ec.europa.eu/eurostat/statistics-explained/extensions/EurostatPDFGenerator/getfile.php?file=188.154.8.42_1474102804_64.pdf.

Guillaume, Thomas, Damris, Muhammad and Kuzyakov, Yakov. 2015. Losses of soil carbon by converting tropical forest to plantations: erosion and decomposition estimates by δ13C. *Global change Biology 21.* 2015, pp. 3548-3560.

Herber, Lawrence. 1969. Separation of feldspar from quartz by flotation. *The american mineralogist 54.* 1969, pp. 1212-1215.

Huges, P.D., Woodward, J.C. and Gibbard, P.L. 2006. Quaternary glacial history of the Mediterranean mountains. *Progress in Physical Geography 30.* 2006, pp. 334-364.

ICS. 2016. International Comission on Stratigraphy (ICS). Subcomission on Quaternary Stratigraphy (SQS). [Online] 2016. [Cited: 9 14, 2016.] http://www.stratigraphy.org.

IPCC. 2013. The Physical Science Basis. Contribution of Working Group I to the Fifth Assessment Report of the Intergovernmental. [book auth.] T.F. Stocker, et al. *Climate Change 2013.* Cambridge, United Kingdom and New York, NY, USA : Cambridge University Press, 2013, pp. 1-203.

Ivy-Ochs, Susan and Kober, Florian. 2008. Surface exposure dating with cosmogenic nuclides. *Quaternary Science Journal 57.* 2008, pp. 157-189.

Johnson, DL. and Watson-Stegner, D. 1987. Evolution model of pedogenesis. *Soil Science 143.* 1987.

Kawatra, S.K. 2011. Fundamental principles on froth floatation. *SME Mining Engeneering Handbook 2.* 2011, pp. 1517-1531.

Kelley, J.M., Bond, L.A. and Beasley, T.M. 1999. Global distribution of Pu isotopes and 237Np. *The Science of the Total Environment 237.* 1999, pp. 483-500.

Ketterer, Michael. 2016. *Cover letter 239/240 Pu results.* Colorado : s.n., 2016.

Ketterer, Michael, et al. 2004. Rapid dating of recent sediments in Loch Ness: inductively coupled plasma mass spectrometric measurements of global fallout plutonium. *Science of the Total Environment 322.* 2004, pp. 221-229.

Köppen, W. 1936. *Das geographische System der Klimate. Handbuch der Klimatologie.* Berlin : Gebrüder Borntraeger, 1936. Vol. 1.

Lal, D. 1988. In situ-produced cosmogenic isotopes in terrestirial rocks. *Annual Review of Earth and Planetary Scienes 16.* 1988, pp. 355-388.

Lal, D., et al. 2013. Applicability of 239Pu as a tracer for soil erosion in the wet-dry tropics of nothern Austalia. *Nuclear Instruments and Methods in Physics Research B 294.* 2013, pp. 577-583.

Le Pera, Emilia and Sorriso-Valvo, Marino. 2000. Weathering and morphogenesis in a Mediterranean climate, Calabria, Italy. *Geomorphology 34.* 2000, pp. 251-270.

Lulli, L. and Vecchio, G. 2000. I suoli delle Tavoletta "Lago Cecita" nella Sila Grande in Clabria. *Monografia Istituto Sperimentale per lo Studio e la Difesa del Suolo, Progetto Panda.* 2000, p. 78 pp.

Lulli, L., et al. 1992. Contributo alla conoscenza dei suoli dell'altopiano Silano: descrizione e commento della carta dei suoli Centro Sperimentale Dimostrativo ESAC di Molarotta, Camigliatello Silano (CS). *Calabria Verde 11.* 1992, pp. 31-42.

Messerli, Bruno. 1967. Die eiszeitliche und die gegenwärtige Vergletscherung im Mittelmeerraum. . *Geographica Helvetica, 22.* 1967, pp. 205-228.

Meusburger, K., et al. 2013. Combined use of stable isotopes and fallout radionuclides as soil erosion indicators in a forested mountain site, South Korea. *Biogeosciences 10.* 2013, pp. 5627-5638.

Olivetti, Valerio, et al. 2012. Uplift history if the Sila Massif, southern Italy, deciphered from cosmogenic 10Be erosion rates and river longitudinal profile analysis. *Tectonics 31.* 2012.

Perri, Francesco, et al. 2014. Characterization of granitoid profiles in the Sila Massif (Calabria, southern Italy) and reconstruction of weathering processes by mineralogy, chemistry, and reaction path modeling. *Journal of Soils and Sediments 15.* 2014, pp. 1351-1372.

Scarciglia, Fabio. 2015. Weathering and exhumation history of the Sila Massif upland plateaus, southern Italy: a geomorphological and pedological perspective. *Soil Sediments 15.* 2015.

Scarciglia, Fabio, et al. 2014. A comparison of Quaternary soil chronosequences from the Ionian and Thyrrhenian coasts of Calabria, southern Italy: Rates of soil development and geomorphic dynamics. *Quaternary International 376.* 2014, pp. 146-162.

Scarciglia, Fabio, et al. 2012. Role of lichens in weathering of granodiorite in the Sila uplands (Calabria, southern Italy). *Sedimentary Geology.* 2012, pp. 119-134.

Scarciglia, Fabio, Le Pera, Emilia and Critelli, Salvatore. 2005. Weatering and pedogenesis in the Sila Grande Massif (Calabria, South Italy): From field scale to micromorphology. *Catena 61.* 2005, pp. 1-29.

Schaller, M., et al. 2002. A 30 000 yr record of erosion rates from cosmogenic 10Be in Middle European river terraces. *Earth adn Planetary Science Letters 204.* 2002.

Schaub, Monika and Alewell, Christine. 2009. Stable carbon isotopes as an indicator for soil degradation in an alpine environment (Urseren Valley, Switzerland). *Rapid Communications in Mass Spectrometry 23.* 2009, pp. 1499-1507.

Sercon. 2016. The Stabel Isotope Company. [Online] 2016. [Cited: May 2, 2016.] http://www.sercongroup.com/sercon/force_download/69.

U.S. NSF National Program. 2016. Critical Zone Observatories. [Online] 2016. http://www.criticalzone.org.

VBBo. 1998. Federal Law. [Online] 1998. https://www.admin.ch/opc/de/classified-compilation/19981783/201604120000/814.12.pdf.

Versace, P., et al. 1989. Valutatione delle piene in Calabria. *Geodata 30.* 1989, p. 232 pp.

Zollinger, Barbara, et al. 2015. The effect of permafrost on time-split soil erosion using radionuclides (137Cs, 239+240Pu, meteoric 10Be) and stable isotopes (δ13C) in the eastern Swiss Alps. *Journal of Soils and Sediments 15.* 2015, pp. 1400-1419.

Appendix

UNIVERSITY OF ZURICH - IRCHEL

DEPARTMENT OF GEOGRAPHY   WINTERTHURERSTRASSE 190   8057 ZURICH

^{10}Be - LABORATORY   Prof Dr. M. Egli   Tel. (044) 635 51 14
                                Dr. D. Brandová   Fax (044) 635 68 48
                                e-mail: brandova@geo.unizh.ch

S A M P L E   F O R M   F O R ^{10}B e - D A T I N G

UZ Be:		Atom / gram	Age (years)	Mean sample age	Moraine age
	^{10}Be				
	^{26}Al				

GENERAL
Please note: Each sample requires its own form.

Surname, first name, title:	Ruppli, Annina
Sample code:	Bo 2 / 460
Locality:	Sila
Latitude:	39° 16' 53'' Longitude: 16° 32' 23'' Altitude (m a.s.l.) 1572
Photos:	DSC_9099
Exposition :	115° N Dip: 80 °
Shielding :	Separate sample form (Bo2/460_Shielding)
Lithology:	Sila Massif
Sampling date:	27.10.2015
Sample thickness:	3 cm
Weight of sample:	1.6 kg
Weight of crushed sample:	
Rock Type:	Granite
Sampling technique	Hammer, chisel, stone saw

Appendix figure 1. Exemplary sample form for ^{10}Be-Dating in the field.

Appendix table 1. Complete results for ^{10}Be measurements and CRONUS calculations.

Sample name	Latitude (DD)	Longitude (DD)	Elevation (m a.s.l.)	Thickness (cm)	Shielding correction	[Be-10] atoms/g	AMS measured error	Erosion rate (cm/yr)	Exposure age (yr)	Uncertainty (yr)
Bo1/10	39.281	16.539	1572	3	0.490	501100	5.93%	0	79'876	6'214
Bo1/25	39.281	16.539	1572	3	0.498	284000	7.43%	0	41'590	3'790
Bo1/76	39.281	16.539	1572	3	0.558	344000	9.91%	0.0001	50'003	5'814
Bo1/102	39.281	16.539	1572	3	0.879	689600	4.06%	0.0001	65'610	4'429
								0.0005	77'961	11'337
Bo1/128	39.281	16.539	1572	3	0.613	306500	4.18%	0.0001	40'248	2'674
								0.0005	42'916	5'307
Bo1/225	39.281	16.539	1572	2	0.999	302370	5.45%	0.0001	24'118	1'798
								0.0005	24'948	3'000
Bo2/-20	39.281	16.540	1572	9.5	0.724	138134	5.23%	0	13'759	1'400
								0.0005	15'316	1'637
Bo2 30	39.281	16.533	1572	3	0.614	69410	20.03%	0.0001	10'724	2'234
								0.0005	10'988	2'546
Bo2/240	39.281	16.540	1572	2	0.771	301304	4.94%	0.0001	31'145	2'219
								0.0005	32'681	3'978
Bo2/460	39.281	16.540	1572	3	0.614	709104	3.86%	0.0001	92'286	6'285
								0.0005	126'678	23'350
Bo2/560	39.281	16.540	1572	2	0.972	1124660	3.92%	0.0001	99'636	6'883
								0.0005	142'727	28'681
Bo3/-20	39.281	16.539	1572	9.5	0.612	167219	5.11%	0	19'614	1'986
								0.0005	21'614	2'301
Bo3/170	39.281	16.539	1572	2	0.998	265423	5.18%	0.0001	21'128	1'526
								0.0005	21'783	2'550

Appendix table 2. Complete soil properties and results on reference site R.

Name		moist sample	dry sample	water content	skeleton content	fine material	soil density	LOI	C$_{tot}$	δ^{13}C	Pu Inventory
		(g)	(g)	(%)	(%)	(g)	g/cm³	(%)	(%)	(‰)	(Bq/m²)
R	1.1	46.4	28.3	8.40	3.16	21.50	0.358	40.42%	19.04	-27.99	7.34
	1.2	66.3	52.9	8.88	3.45	47.70	0.795	16.80%	6.17	-26.80	13.61
	1.3	73.3	60.1	9.68	4.54	53.90	0.898	16.44%	5.10	-26.28	12.26
	1.4	80.5	67.3	10.63	6.92	58.70	0.978	16.16%	5.46	-26.34	17.68
	1.5	71.1	55.7	10.95	3.98	50.10	0.835	15.26%	5.34	-26.37	13.43
	2.1	48.3	31.8	7.97	2.80	26.00	0.433	25.66%	10.82	-27.74	9.53
	2.2	67.3	51.7	10.50	4.98	44.30	0.738	19.62%	7.42	-26.93	18.31
	2.3	68.7	53	10.79	4.40	46.60	0.777	17.09%	6.58	-26.74	16.04
	2.4	67.7	53.1	9.88	3.79	47.50	0.792	22.26%	6.01	-26.55	18.60
	2.5	78	60.4	13.73	7.57	50.70	0.845	16.58%	5.96	-26.55	24.23
	3.1	46.1	30	7.42	7.61	13.50	0.225	28.63%	12.79	-27.89	4.19
	3.2	90.3	71.5	16.98	9.93	60.50	1.008	17.20%	5.95	-26.69	16.76
	3.3	65	52.7	8.00	5.14	44.80	0.747	16.65%	5.54	-26.34	14.20
	3.4	86	67	16.34	8.34	57.30	0.955	15.69%	5.12	-26.33	24.87
	3.5	72.3	56.5	11.42	7.30	46.40	0.773	18.85%	6.80	-26.52	31.63
	4.1	39.1	23	6.30	1.96	18.00	0.300	39.88%	18.78	-28.10	5.60
	4.2	77.3	59.8	13.53	6.18	51.80	0.863	17.45%	6.28	-26.85	10.12
	4.3	73.6	57.5	11.85	5.52	50.00	0.833	14.63%	4.75	-25.95	6.06
	4.4	82.1	65.8	13.38	7.96	56.10	0.935	14.68%	4.73	-26.07	9.03
	4.5	85.7	64.5	18.17	6.17	57.30	0.955	15.08%	4.91	-26.60	13.25

*Appendix table 3. Complete soil properties and results on investigation site A.*

Name		moist sample	dry sample	water content	skeleton content	fine material	soil density	LOI	C_{tot}	$\delta^{13}C$	Pu Inventory
		(g)	(g)	(%)	(%)	(g)	g/cm³	(%)	(%)	(‰)	(Bq/m²)
A	1.1	56.6	44.2	7.02	2.77	39.30	0.655	17.26%	7.00	-27.96	4.54
	1.2	93.6	85.1	7.96	15.07	69.00	1.150	9.31%	2.55	-26.90	9.69
	1.3	67	61	4.02	7.71	49.50	0.825	8.65%	2.21	-26.59	8.03
	1.4	62.1	58.3	2.36	6.33	48.10	0.802	7.17%	1.62	-26.30	6.54
	1.5	76.6	70.3	4.83	11.41	55.40	0.923	8.42%	1.92	-26.06	10.69
	2.1	70.6	58.7	8.40	8.90	46.10	0.768	13.87%	5.54	-28.43	2.80
	2.2	67.7	62.3	3.66	10.76	46.40	0.773	7.71%	1.93	-25.75	4.97
	2.3	51.1	48.4	1.38	6.08	36.50	0.608	7.23%	1.65	-26.33	3.51
	2.4	78.8	75	2.99	18.05	52.10	0.868	7.33%	1.57	-26.32	5.34
	2.5	83.9	78.6	4.45	15.94	59.60	0.993	6.54%	1.09	-25.65	2.71
	3.1	60.4	49.3	6.70	7.79	36.40	0.607	14.05%	5.10	-27.90	3.92
	3.2	83.3	57.8	21.24	15.16	39.60	0.660	7.65%	1.77	-26.44	4.12
	3.3	68.7	62.2	4.47	10.37	47.10	0.785	7.53%	1.63	-26.33	5.16
	3.4	103.5	94.3	9.52	21.63	73.40	1.223	7.46%	1.76	-25.91	8.76
	3.5	69.4	65.2	2.91	11.59	48.50	0.808	7.20%	1.54	-25.89	3.93
	4.1	53.8	41.3	6.73	2.53	36.60	0.610	17.96%	7.44	-28.19	4.02
	4.2	70.5	64.4	4.30	10.01	50.20	0.837	8.00%	1.95	-26.76	4.14
	4.3	69.6	63.9	3.97	8.28	52.00	0.867	7.56%	1.70	-26.48	5.78
	4.4	86.3	77.9	7.25	13.72	62.00	1.033	7.17%	1.49	-25.86	8.00
	4.5	77	70.5	5.01	11.86	55.10	0.918	7.33%	1.59	-25.20	7.82

Appendix table 4. Complete soil properties and results on investigation site B.

Name		moist sample (g)	dry sample (g)	water content (%)	skeleton content (%)	fine material (g)	soil density g/cm³	LOI (%)	C$_{tot}$ (%)	δ^{13}C (‰)	Pu Inventory (Bq/m²)
B	1.1	42.4	30.1	5.22	1.53	26.50	0.442	20.42%	8.47	-28.30	2.82
	1.2	93.6	80.4	12.36	14.23	65.20	1.087	9.25%	2.34	-26.70	3.42
	1.3	79.7	72.7	5.58	11.96	57.70	0.962	7.88%	1.72	-25.63	7.90
	1.4	86.7	79.8	5.98	15.95	61.40	1.023	7.06%	1.12	-25.54	7.10
	1.5	73.2	67.7	4.03	11.64	51.80	0.863	6.67%	1.22	-25.33	5.72
	2.1	37.4	27.2	3.81	1.83	22.30	0.372	24.00%	10.44	-28.18	2.53
	2.2	77.9	66.7	8.72	12.78	50.30	0.838	10.92%	3.42	-27.10	5.76
	2.3	70.8	64.8	4.25	11.26	48.90	0.815	7.88%	1.52	-25.86	6.20
	2.4	87	80.9	5.31	16.88	61.50	1.025	7.70%	1.46	-25.47	8.25
	2.5	75.2	70.1	3.84	12.78	53.10	0.885	6.91%	1.40	-25.48	5.93
	3.1	70.7	56.1	10.32	6.15	47.40	0.790	13.88%	4.84	-27.76	5.01
	3.2	91.7	81	9.81	16.23	63.30	1.055	8.42%	1.94	-26.31	7.02
	3.3	72.4	66.8	4.05	12.16	50.00	0.833	8.15%	1.66	-25.73	5.05
	3.4	97.2	91.5	5.54	17.30	73.70	1.228	7.74%	1.52	-25.53	11.12
	3.5	73.7	67.3	4.72	11.35	51.90	0.865	7.81%	1.51	-25.75	6.75
	4.1	44.1	32.3	5.20	2.47	26.70	0.445	19.48%	8.19	-28.11	2.82
	4.2	63	57.5	3.47	7.69	45.30	0.755	9.82%	2.44	-26.67	4.67
	4.3	73.7	64.7	6.63	10.47	50.50	0.842	9.27%	2.34	-25.82	2.11
	4.4	98.4	87.8	10.43	18.79	68.70	1.145	8.09%	1.71	-25.54	5.69
	4.5	72.8	67.4	3.93	10.41	53.10	0.885	7.84%	1.50	-25.25	6.90

Appendix table 5. Derived surface lowering and soil erosion rates for boulder 2, calculated for minimal rock erosion (= 0.0001 cm/yr) and maximal rock erosion (= 0.0005 cm/yr).

Age (yr BP)	min. rock erosion surface lowering (mm/yr)	erosion rates (t/ km²/yr)	Max. rock erosion surface lowering (mm/yr)	erosion rates (t/ km²/yr)
100	0.173	141	0.142	116
1'000	0.167	136	0.139	113
2'000	0.160	130	0.135	110
3'000	0.154	125	0.132	108
4'000	0.147	120	0.129	105
5'000	0.141	115	0.125	102
6'000	0.135	110	0.122	99
7'000	0.130	106	0.119	97
8'000	0.124	101	0.115	94
9'000	0.118	97	0.112	91
10'000	0.113	92	0.109	89
15'000	0.088	72	0.094	77
20'000	0.067	55	0.080	65
25'000	0.050	41	0.068	55
30'000	0.036	29	0.056	46
35'000	0.026	21	0.046	38
40'000	0.019	16	0.037	30
45'000	0.016	13	0.029	24
50'000	0.017	14	0.022	18
55'000	0.021	17	0.017	14
60'000	0.029	23	0.013	10
65'000	0.040	33	0.009	8
70'000	0.055	45	0.007	6
75'000	0.074	60	0.007	5
80'000	0.096	78	0.007	6
85'000	0.122	99	0.009	7
90'000	0.151	123	0.011	9
95'000	0.184	150	0.015	12
100'000	0.220	180	0.020	17
105'000	0.261	212	0.027	22
110'000	0.304	248	0.034	28
115'000	0.352	287	0.043	35
120'000	0.403	328	0.052	43
125'000	0.457	373	0.063	52
130'000	0.516	420	0.076	62
135'000	0.578	471	0.089	72
140'000	0.643	524	0.103	84
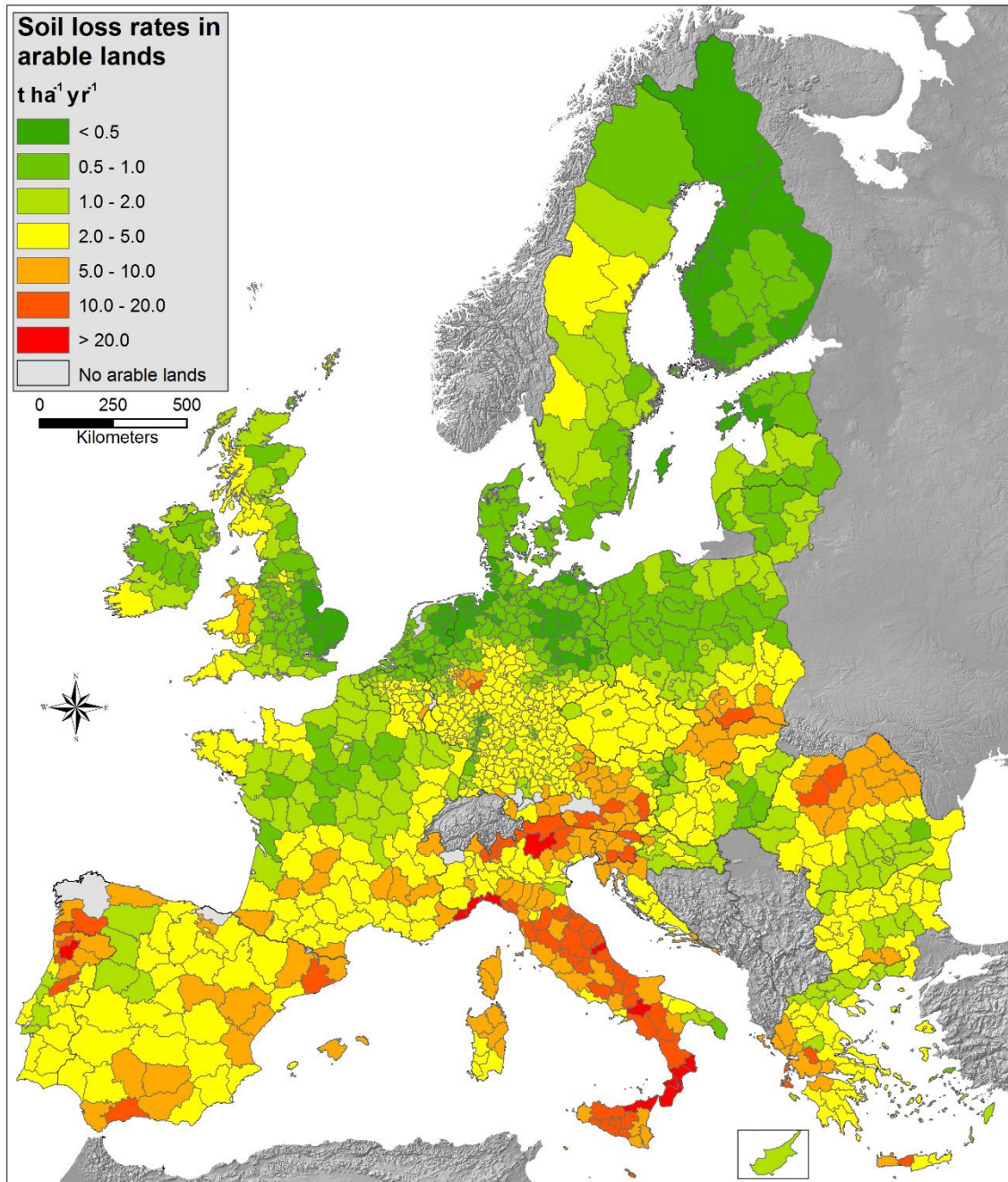
Appendix figure 2. Complete figure about soil loss rates in Europe from Eurostat, 2015, online available: http://ec.europa.eu/eurostat/statistics-explained/index.php/Agri-environmental_indicator_-_soil_erosion

Appendix figure 3. Global chronostratigraphical correlation table for the last 2.7 million years. Edition from 2016. Online available: http://www.stratigraphy.org/index.php/ics-chart-timescale

H

Personal declaration

I hereby declare that the submitted thesis is the result of my own, independent work. All external sources are explicitly acknowledged in the thesis.

Zurich, September 2016

Annina Ruppli